

THE EVALUATION OF CHEMICAL WEAR ON SINGLE CRYSTAL DIAMOND
TOOLS WHILE DIAMOND TURNING A BINARY Cu-Ni ALLOY SYSTEM

by

Eric Calmer Browy

A thesis submitted to the faculty of
The University of North Carolina at Charlotte
in partial fulfillment of the requirements
for the degree of Master of Science in
Optical Science and Engineering

Charlotte

2014

Approved by:

Dr. Chris Evans

Dr. Steve Patterson

Dr. Brigid Mullany

ABSTRACT

ERIC CALMER BROWY. The evaluation of chemical wear on single crystal diamond tools while diamond turning a binary Cu-Ni alloy system. (Under the direction of DR. CHRISTOPHER J. EVANS)

The current work describes the evaluation of chemical wear on diamond tools while diamond turning copper nickel alloys of varying composition. The primary goal of my project is to quantify the chemical wear of single crystal diamond tools while diamond turning Cu-Ni alloys of different compositions. Pure copper is commonly understood to give negligible tool wear, while pure nickel is reported to give rapid wear. The Cu-Ni equilibrium phase diagram shows a single phase at all compositions. The development and testing of a method to evaluate and quantify diamond tool wear is also described within the current work. The method chosen for development is the metrology of the progressive edge recession of the diamond. A procedure of progressive plunge cuts into an ultra-bright acid copper before and after diamond turning of the workpiece takes a snapshot of the edge of the diamond tool as the cutting distance increases. An algorithm executed in MatLab® displays the residual tool wear after removal of the initial diamond tool geometry. A theoretical model has been developed to predict the chemical diamond tool wear and the results will be shown within the body of work.

ACKNOWLEDGMENTS

I would like to thank Dr. Chris Evans, for the unwavering support and patient guidance as I worked to better myself and understanding of the world. I would also like to thank Drs. Brigid Mullany and Jimmie Miller for igniting a passion and giving me the opportunity to realize it. I would also like to thank Dr. Ed Paul for his contributions and guidance during this project. To my peers in the Center for Precision Metrology, thank you for participating in a collaborative environment, where we have all grown and benefited.

Above all else I would like to thank my parents Ann and Eric Herold, who have been a constant source of stability and mentors through all of my challenges, believing in me and in my ability to reach my goals. Finally, to Carmel Bemus a thank you for the daily love and support towards following my passions.

TABLE OF CONTENTS

LIST OF TABLES	vii
LIST OF FIGURES	viii
CHAPTER 1: INTRODUCTION	1
CHAPTER 2: BACKGROUND	5
2.1 Mechanisms of Diamond Tool Wear	5
2.2 Materials used for Diamond Turning	6
2.3 Diamond Tool Wear Measurement	8
CHAPTER 3: EXPERIMENTAL METHODS	10
3.1 Scanning White-Light Interferometry	13
3.2 Edge-Recession and Surface Finish	14
3.3 Metrology Methods and Experimental Setup	15
3.4 Experimental Terminology	19
3.5 Experimental Parameters and Conditions	22
3.6 Direct and Indirect Tool Wear Metrology	26
CHAPTER 4: MATERIAL CONSIDERATIONS	34
4.1 Effective D-index	35
4.2 Materials of Interest	36
CHAPTER 5: RESULTS AND DISCUSSION	39
5.1 Copper Witness Sample	39
5.2 Diamond Tool Wear Categories	41
5.3 Alloys of Varying Composition	45
5.4 Feedrate Testing	50

5.5	Variation of Surface Velocity	54
5.6	Constant Time Testing	57
5.7	Uncertainty	58
CHAPTER 6: CONCLUSIONS AND FUTURE WORK		61
REFERENCES		63
APPENDIX: MATLAB CODE		66

LIST OF TABLES

TABLE 3.1: Variables used to describe the parameters selected during the testing of chemical diamond tool wear	22
TABLE 3.2: The parameter space for the initial set of tests in order to test the d-index theory	23
TABLE 3.3: The parameter space for the short run tests to increase the resolution of the wear in the diamond tool	24
TABLE 3.4: The parameters under test for the variation of surface speed testing, which also varies the cutting time	25
TABLE 3.5: Testing holding the surface speed and varying the feedrate during turning Monel	25
TABLE 3.6: The tests holding the feedrate constant while varying the surface speed on Monel	25
TABLE 4.1: The tested alloys by nominal composition from manufacture certifications, and the nominal effective d-index	36
TABLE 5.1: The Percent weight composition of Cu-Ni alloys, as measured by Energy-dispersive X-ray Spectroscopy (EDS)	49

LIST OF FIGURES

FIGURE 3.1: Wear scar and VB MAX of 15 μ m/revolution test	10
FIGURE 3.2: An illustration of the general process for measuring the edge recession of the diamond tool while single point diamond turning Cu-Ni alloys	12
FIGURE 3.3: A general illustration of the experimental tool wear measurement, in order to quantify the diamond tool wear	13
FIGURE 3.4: The final stepped concentric workpiece after a test (left) with 5 micrometer depths of cut. The measurement of the each step (right) to determine the RMS of the surface at the prescribed cutting distances	15
FIGURE 3.5: An illustration of the top view of the experimental setup used in testing	16
FIGURE 3.6: A profilometer trace of the UBAC witness sample illustrating the visible change in plunge depth	18
FIGURE 3.7: A schematic illustration of the stepped concentric workpiece after testing	19
FIGURE 3.8: A schematic of the annulus removed by the diamond tool, and the variables associated with each band	20
FIGURE 3.9: The Area RMS (Sq) of the stepped concentric workpiece plotted versus the Cutting distance	27
FIGURE 3.10: The raw data from the ZeGage TM in .dat form (left) converted to the Matlab variable as a three dimensional matrix of points (right)	28
FIGURE 3.11: The raw plunge data (left) is rotated, aligning the plunges for subsequent steps (right)	29
FIGURE 3.12: The rotated data (left) is tilt corrected (right) by fitting a plane to the flats and subtracting it	29

FIGURE 3.13: The rotation and tilt corrected image, (top left) the same plunge with the flats removed. (top right) The plunge is averaged down the columns creating an average profile of 1024 rows, un-centered (bottom left). The plunge is then centered about zero by using the uncut area of the plunge (bottom right)	31
FIGURE 3.14: The replication of the unworn tool and the final plunge for the diamond tool wear experiment for selection of the left and right limits, and subsequent subtraction of the initial tool shape from the final plunge	32
FIGURE 3.15: The residual of the subtraction of the two plunges, the initial plunge (bottom) and the final plunge (top)	32
FIGURE 3.16: The final aligned residual of the initial plunge and the final plunge after tilt correction	33
FIGURE 4.1 Cu-Ni Phase diagram showing the solid solution of across the range of compositions ⁷	35
FIGURE 4.2: The d-electron index versus the Ni wt%, when the Ni content corresponds with a d-index value of 10 or lower the chemical wear is predicted	38
FIGURE 5.1: The OFHC copper ring caused pieces of diamond to be knocked out on the trailing edge during testing	40
FIGURE 5.2: Duplication of replication process in the diamond tool wear testing in the Cu witness sample. The Left figure on the same scale as other residual plots, and the right with a smaller vertical scale (nm)	41
FIGURE 5.3: The edge recession of the diamond tool nose gives proof that as the cutting distance and time increase the diamond tool wear also increases	42
FIGURE 5.4: The Pekalharing grooves with a 2 μm period in the diamond tools, through a high pass filter with a 4 μm cutoff (0.41 $\mu\text{m}/\text{pixel}$)	43
FIGURE 5.5: Cu70Ni30 (left) an alloy expected to hover around the critical d-index value of 10, has some edge recession, but a lower amount than the edge recession of the Monel (right) which has a lower d-index and thus more leading edge chemical wear	44

FIGURE 5.6: The residuals with a fit quadratic removed from the unworn tool (left), and the same quadratic added into the residuals	45
FIGURE 5.7: The residuals (left) of the diamond tool wear test using pure Ni, and area RMS surface finish versus Cutting Distance (right) which shows the final surface finish greater 100 nm	46
FIGURE 5.8: The residuals (left) of the diamond tool wear test using Monel, a Cu-Ni alloy with the second lowest d-index and second highest amount of wear tested. The RMS versus Cutting Distance (right) shows an increase of roughness as the diamond tool edge recession increases	46
FIGURE 5.9: The residuals (left) of the diamond tool wear test using Constantan, a Cu-Ni alloy with the third lowest d-index. The RMS versus Cutting Distance (right) shows an increase of roughness with diamond tool edge recession	46
FIGURE 5.10: The residuals (left) of the diamond tool wear test using Cu70Ni30, a Cu-Ni alloy with the fourth lowest d-index, which has a d-index that is around the critical value dependent on the trace elements in the alloy. The RMS versus Cutting Distance (right) shows an increase of roughness as the diamond tool edge recession increases	47
FIGURE 5.11: The residuals of the 10 Pence coin (left) and the RMS versus Cutting distance of the workpiece (right)	47
FIGURE 5.12: Shows the residuals of the highest d-indexed Cu-Ni alloy tested (left), and the RMS versus Cutting Distance (right)	48
FIGURE 5.13: The combined final residual of each alloy, with an emphasis on the less aggressive diamond tool wearing alloys highlighted on the right	50
FIGURE 5.14: The residuals and surface finish vs. cutting distance of diamond turned Monel with a spindle speed of 1000 RPM and a Feedrate of 5 micrometers a revolution	51
FIGURE 5.15: The residuals and surface finish vs. cutting distance of diamond turned Monel with a spindle speed of 1000 RPM and a Feedrate of 10 micrometers a revolution	51
FIGURE 5.16: The residuals and surface finish vs. cutting distance of diamond turned Monel with a spindle speed of 1000 RPM and a Feedrate of 15 micrometers a revolution	52

FIGURE 5.17: The combined Final Plunges of the diamond tool wear residuals and combined RMS vs. Cutting Distance	52
FIGURE 5.18: The Crater wear of the diamond tool while conducting the 5 micrometer per revolution test on Monel	53
FIGURE 5.19: The rake face of the four diamond tools used for each feedrate variation (left) with the height in nanometers, and a profile taken across the deepest point of the crater in each tool normal to the cutting edge (right)	54
FIGURE 5.20: The crater wear on the rake face of the diamond tool with height in nanometers (left), and a profile across the most deep section of the crater (right)	55
FIGURE 5.21: Residuals and RMS of Monel turned with 500 RPM Spindle speed and a feedrate of $2\mu\text{m/rev}$	55
FIGURE 5.22: Residuals and RMS of Monel turned with 2000 RPM Spindle speed and a feedrate of $2\mu\text{m/rev}$	56
FIGURE 5.23: Residuals and RMS of Monel turned with varying surface speeds at a feed rate of $2\mu\text{m/rev}$	56
FIGURE 5.24: Residuals and RMS of Monel turned with 500 RPM Spindle speed and a feedrate of $4\mu\text{m/rev}$	57
FIGURE 5.25: Residuals and RMS of Monel turned with 2000 RPM Spindle speed and a feedrate of $1\mu\text{m/rev}$	58
FIGURE 5.26: Combined Residuals and RMS vs. Cutting Distance of constant time tests in Monel	58
FIGURE 5.27: The minimum, maximum, and average difference of measurements at different locations on the witness sample giving a total standard deviation of the location on the witness sample of 1.9 nanometers	59
FIGURE 5.28: A qualitative correlation of the wear scar seen in an SEM next to residual of the same test	60

CHAPTER 1: INTRODUCTION

Single point diamond tools, when used in conjunction with precision machinery can produce optical quality surfaces in both ductile and brittle surfaces. When diamond tools are used instead of conventional turning tools on specialized precision lathes this is referred to as diamond turning. Diamond turning can be used as a process to achieve a final optical surface, or a diamond turned surface can be post-polished to remove the cusp structures, effectively reducing scatter¹ and sometimes to improve surface form.

The process of diamond turning has been used in the modern manner since World War II, to make IR optics for the military². Diamond turning has since matured to be an instrumental step in many precision optical fabrication processes. In many situations diamond tools wear during the cutting process, and due to the high price per diamond tool it is essential to only diamond turn materials which do not rapidly cause diamond tool wear. Many refer to a material as “diamond turnable” meaning that the wear rate on the diamond tool is low enough that a reasonable amount of specular surface can be produced economically³.

Even materials considered “diamond turnable” cause diamond tool wear, leading to an increase in cutting forces, increased surface roughness, and surface form errors. The wear rate depends on the material being cut, diamond tool characteristics⁴, and the wear mechanisms. The result is different wear rates for different materials. Although diamond turning is a mature process, the diamond tool wear has not been quantified for many

materials, especially alloys. In fact there are only qualitative approaches to diamond tool wear prediction. During the development of optimal materials and electroless nickel plating for diamond turning applications, some alloy compositions have been found to produce little diamond tool wear, while others with only slightly different compositions wear diamond tools more rapidly⁵. Chemical wear of the diamond tool is expected to be a function of a large number of variables, including surface speed, chip thickness, diamond orientation, lubricant, workpiece mechanical properties (especially hardness) and chemical composition. Expressed differently, chemical wear rates depend on local temperature and composition.

Cu, a ductile material that provides negligible wear on diamond tools while Ni, adjacent to Cu on the periodic table, rapidly wears diamond tools. Cu-Ni alloys are single phased at all compositions (for equilibrium conditions). This single phase at different compositions allows tests to be completed which vary the Ni content without adding abrasive second phases. Paul et al. and the unpaired d-shell hypothesis⁷ for the onset of chemical wear has been extended to simple alloy systems¹⁴ using the idea of an equivalent unpaired d-shell index. Ignoring trace amounts of manganese and iron commonly found in Cu-Ni alloys, the theory being tested suggests that once a critical Ni content is reached (33 wt% Ni), diamond tools will wear chemically. The purpose of the work described here is to test that theory. Wear rates are complex functions of many variables.

The current methods of diamond tool wear characterization involve removing the diamond tool from the diamond turning machine (DTM) in order to inspect the leading edge where the diamond contacts the workpiece. This can prove to be problematic in

measuring progressive wear due to relocation of the tool into the DTM. In this work a method for in situ diamond tool wear measurements has been developed, and is described in detail in Chapter 3. Briefly, a copper witness sample and the sample under test are both mounted on the spindle of the diamond turning machine.

The diamond tool can be slowly plunge-cut into the copper witness sample which effectively provides a replica of the state of the edge tool at any time. The initial geometry of the single crystal diamond tool is recorded before each experiment. Once the initial plunge-cut is made the face of the workpiece will be turned over a specific distance before a second plunge cut is made. The difference between “before” and “after” plunge cuts into the Cu sample captures the wear over that period. The procedure and analysis is discussed in detail in Chapter 3. By careful selection of the machining conditions, we can retain a small area of the surface generated at well-defined stages in tool wear evolution for subsequent analysis as well the information on the tool edge condition. After a series of tests, the copper witness sample is removed from the diamond turning machine, and the plunge-cut will be measured using a profilometer or a coherence scanning interferometer (CSI). The edge recession as a function of cutting distance or volume provides details on the evolution of wear. Alternatively, the edge recession can be converted to volume removed using the nominal tool geometry.

The binary equilibrium phase diagram for Cu-Ni⁷ shows a single phase at all compositions and no intermetallics. All commercially available alloys have Mn and Fe. Material analysis (described in Chapter 4) qualifies the composition of each alloy and properties of interest. Chapter 5 presents details on the tool wear experimental method

and results for Cu-Ni alloys with nominal copper contents ranging from 90 wt% to 35 wt%. Chapter 6 presents conclusions and suggestions for future work.

CHAPTER 2: BACKGROUND

Diamond tooling is used for many different processes in modern manufacturing. A range of mirrors and transmissive components from precision optics to rolls for fabricating reflective safety vests are finished with single crystal diamond end mills or diamond turning tools. These single crystal diamonds are expensive and rapid tool wear can add significant expense to individual optics and make some components (for example large drum rolls) difficult or impossible to make to tolerance. The symptoms of tool wear are well understood in industry, where materials are often described as “diamond turnable”^{1, 3}. There is a substantial body of literature on diamond wear in general, and somewhat less in the specific area of single crystal diamond tool wear. In particular there is no good method for predicting the chemical wear of diamond tools when machining alloys. This thesis describes experimental work that will be used to develop and refine such predictive methods.

2.1 Mechanisms of Diamond Tool Wear

It is well known that diamond turning ferrous materials rapidly wears diamond tools, but the tool wear mechanisms are not well understood. Evans³ described various mechanisms for diamond tool wear, dividing them into adhesion, abrasion, tribothermal and tribochemical wear, noting that multiple mechanism might apply simultaneously. That paper and Paul et al⁶ together provide an extensive literature review which will not be repeated here.

Adhesive wear is attributed to an unstable built up edge on the diamond tool, resulting in diamond fracture due to an increase in tensile forces on the diamond tool edge. Diamond tools are lapped and polished with great care when creating the diamond tool edge. When the tool edge is in contact with the workpiece, micro-cleavage may result from the sub-surface damage, perhaps also affected by fatigue. Diamond fracture strength has been shown to decrease with the number of stress cycles⁸. The number of stress cycles to initiate material removal may explain aspects of abrasive wear.

Tribothermal wear is caused when there is an increase in temperature at the tool workpiece interface, initializing graphitization of the diamond tool. The peak temperatures are just behind the tool edge on the rake face, causing crater wear. Elevated temperatures are also found at the tool edge and down the clearance. During single point diamond turning temperatures⁹ appear to be well below the requirements for rapid graphitization of diamonds. Tribochemical wear describes cases where catalyzed carbon-carbon bond breaking takes place at temperatures well below the graphitization temperature. Oxidation¹⁰, diffusion and catalyzed graphitization have all been discussed in the literature. From the perspective of tool diamond wear, it does not matter much what happens after carbon-carbon bond breaking in the diamond.

2.2 Materials used for Diamond Turning

A significant body of experimental work has been compiled in tabulations of materials which are “diamond turnable” and which are not. The meaning of “diamond turnable” is open to discussion, but may be taken to mean a material which an “optical surface” can be obtained over a reasonable area.

Aluminum, for example, is widely diamond turned for a variety of applications. However, not all aluminums are equal. Some alloys cause tool wear, presumably caused by hard second phases (silicates) or other contaminants. The result is poor surface finish, both from the interactions of the diamonds with the particles, and “orange peel” (grain relief) when cutting forces increase from dull, worn edges on the tools.

Electroless nickel is another material that has given low wear in diamond turning of some compositions and heat treatments and high wear in others. The group at Lawrence Livermore National Laboratory (Dini, Donaldson, Syn and Taylor) undertook a systematic study suggesting an optimum of low wear and high hardness can be achieved on electroless nickel (eNi), held at 200°C for 2 hours for heat treatment with 10 wt% phosphorous¹¹. Higher temperature heat treatment (600°C) is not recommended due to the association with lower hardness, increased grain size, cutting force, tool wear, and surface roughness. Another option to electroless nickel is electroplated nickel, which has similar metallurgical characteristics independent of the deposition process. The electroplated nickel can contain a higher wt% phosphorous, decreasing the total diamond tool wear¹².

Paul et al.⁶ addressed the chemical aspects of diamond tool wear, showing a relationship between the number of unpaired d-shell electrons in the element and tool wear. They also suggest an explanation why nickel, a material which causes significant diamond tool wear, when alloyed with phosphorous can produce low amounts of diamond tool wear, and excellent optical quality surfaces. “Electroless nickel is actually a nickel-phosphorus Alloy in which unpaired d-electrons from nickel atoms become paired with p-electrons from phosphorus atoms. Because the resulting alloy has fewer free

unpaired d-electrons, it forms fewer complexes with the carbon atoms in the diamond tool, and chemical tool wear is substantially reduced.”⁶ It should be noted that this explanation applies only to the metastable amorphous single phase coating deposited from high phosphorous plating baths. High temperature heat treatment transforms this into crystalline nickel (<4% P) with hard nickel-phosphides on the grain boundaries¹³.

The National Science Foundation¹⁴ project funding the current work stems from this observation. There a d-index value is proposed for alloys based on the idea (suggested above) that appropriate p- and s-shell electrons may combine with d-shell electrons to give a conduction band with no apparent vacancies to catalyze bond breakage. Computation of the d-index is further detailed in Chapter 3. The implication of this is that chemical diamond tool wear may be predicted for any single phased alloy, or for different phases in a multi-phased alloy. The tool wear will never be zero, as the other mechanisms may still be active. Testing the theory requires a method to measure tool wear intermittently during a cutting test with minimal disturbance.

2.3 Diamond Tool Wear Measurement

Tool wear typically results in deterioration of the surface finish. Thus, and indirect measure of wear is change in the surface finish measurements as a function of cutting distance. In order to do this Taylor et al.¹¹, face-turned a stepped concentric work piece, allowing for progressive surface finish values, to determine how the workpiece changed relative to the diamond tool wear. In order to determine the diamond tool wear while face turning eNi plated mirrors Taylor et al. plunge-cut the diamond tool into a fine grained copper to replicate the tool edge in the copper. A talystep stylus profilometer was used to trace a profile across the plunge cuts to obtain progressive edge-recession of the

diamond tool. This method has an inherent cosine error associated with it, due to alignment issues while using a stylus profilometer, but provide a good indication of the evolution of the tool edge. Evans¹⁴ replicated this method in Udylite Bright Acid Copper (UBAC) obtaining the same progressive diamond tool edge-recession replicated with a plunge-cut as tool wear increases.

Shi et al.¹⁵ took another approach to measuring diamond tool wear. On the cutting edge of the diamond tool which separates the rake and flank face, a line is drawn with electron-beam-induced deposition (EBID) of carbon in an SEM. The contrast gained in a field emission Scanning Electron Microscope (SEM) operation allows the user to extract high-resolution results of the tool edge. This method proved to be a reasonable measurement of tool wear with several reported contributors to uncertainty in the measurement, but requires to tool to be removed from the machine and, hence is inappropriate for following the progression of wear in a single tool.

Prior work at UNC Charlotte¹⁶ extended the plunge cut technique using area based methods (i.e. scanning white light interferometry). That work is further developed here (see Chapter 3), providing a method with higher resolution and lower associated uncertainty than previous methods. This will allow for trends in the tool wear mechanisms to be studied, resulting in better understanding of diamond tool wear.

CHAPTER 3: EXPERIMENTAL METHODS

Quantification of tool wear in single crystal diamond tools used for ultra-precision machining is notoriously difficult. Much of the literature uses indirect measures, such as the change in surface finish with cutting distance¹¹. This approach provides a functionally relevant metric, but makes it difficult to gain fundamental insight into the wear mechanism. A number of workers have used scanning electron microscopy to observe directly the wear on the tool¹⁷ and characterize it using ISO standard parameters such as V_B (flank wear, see ISO 3685 (1993)) or $V_B \text{ max}$ as seen in Figure 3.1.

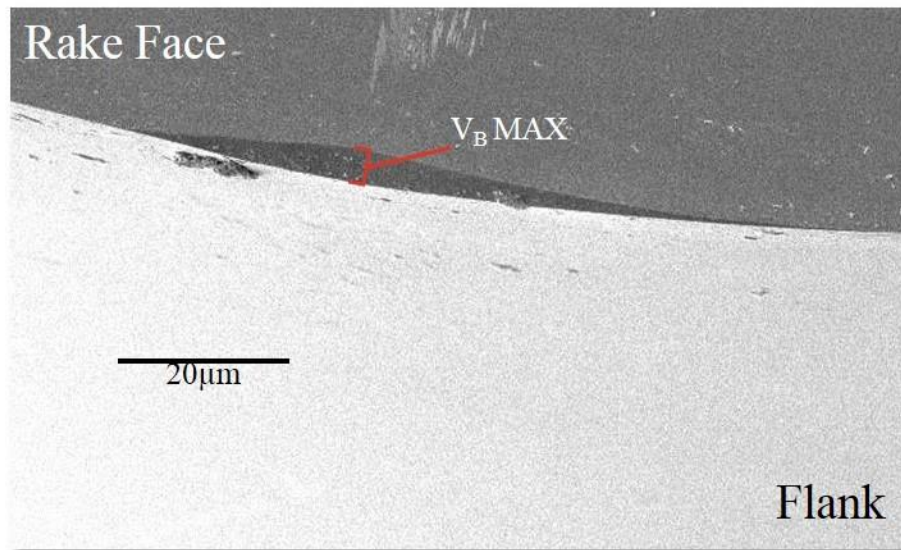


Figure 3.1: Wear scar and $V_B \text{ MAX}$ of 15 μm /revolution test

This approach is adequate when the tool edge recession is large. Consider a 6° clearance, zero degree rake tool with 0.1 micrometer edge recession normal to the rake.

The “wear scar” will extend 3 micrometers from the intersection of rake and clearance for the test conducted on the above diamond tool. Dow and his students¹⁵ have used the SEM to write a carbon “line” nominally normal to the cutting edge running from rake to clearance. Tilting the tool and imaging the distortion of the line provides a means of characterizing the tool shape. These approaches require that the tool be removed from the machine and over coated (typically with gold-palladium) to avoid charging. Relocating the tool after inspection would be difficult with standard tools and tool holders.

This chapter describes a development of the plunge cut replication method developed (seemingly in parallel) by Hurt et al at the Naval Weapons Center at China Lake, CA and Syn, Donaldson, Taylor et al at Lawrence Livermore National Laboratory, Livermore CA^{11, 18}. They slowly fed the tool into a previously diamond tuned surface of a copper sample to make a “replica” of the tool edge. Deterioration of the edge quality was observed using high resolution profilometer traces (Talystep) or by Nomarski differential interference contrast (DIC) microscopy. Adam Griffin¹⁶ measured fly-cut plunges into a copper sample using a scanning white light interferometer, and subtracted the “new” tool plunge from a number of subsequent plunges after cycles of single point diamond fly-cutting on materials expected to wear the tool. That approach has been refined and applied to face turning. Figure 3.2 below is an illustration of the diamond tool replication process.

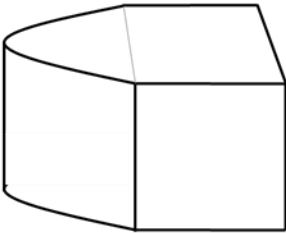
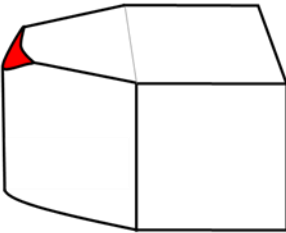



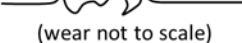
	Unworn Diamond	Worn Diamond
Illustration of diamond tool tip		
Replica of diamond tool edge		
Residual of tool edge		

Figure 3.2: An illustration of the general process for measuring the edge recession of the diamond tool while single point diamond turning Cu-Ni alloys.

In order to determine the effect of variations of composition in the Cu-Ni alloys on single crystal diamond tools, a repeatable method must be used to measure progressive edge recession of the diamond tool with cutting distance. For face turning a sample of the workpiece material is mounted on the spindle on-axis. A ring of “replica” metal (copper) surrounds the workpiece. Once the system is set up, a plunge is made into the copper (rotating) to encode the shape of the new tool. Next the tool is used to machine the workpiece over a prescribed interval before a second plunge is made. This process is repeated a number of times, generating a series of replications of the tool edge profile. At the end of a test, the plunges for each step in the cutting test are measured with a scanning white light interferometer (SWLI). The height map of each replica is exported and processed in Matlab, as described in Section 3.6. Figure 3.3 is a general illustration of the procedure to quantify the wear process.

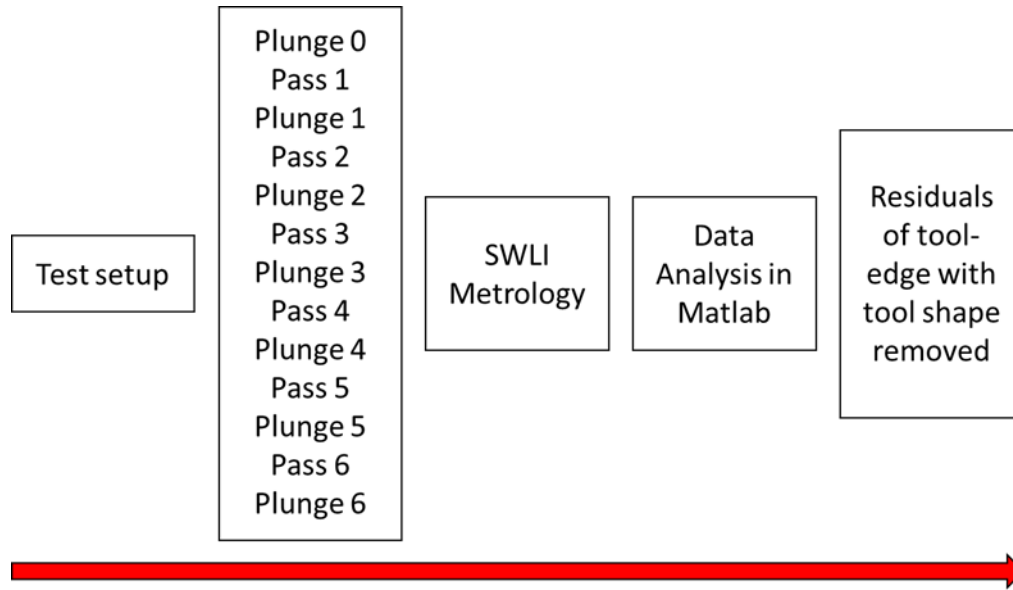


Figure 3.3: A general illustration of the experimental tool wear measurement in order to quantify the diamond tool wear.

3.1 Scanning White Light Interferometry

The majority of the data reported here were obtained using a Zygo ZeGageTM environmentally tolerant Scanning White Light Interferometer (SWLI) located adjacent to the diamond turning machine. The operating principles for SWLI are described, inter alia, by de Groot¹⁹.

Vibrational tolerance of this instruments has been documented²⁰, along with the correlation to profilometry measurements under laboratory conditions²¹. Measurements at UNCC²² indicate noise per pixel of 2 nm Root Mean Square (RMS) for a single scan of the microscope objective. Averaging multiple scans reduces this Type A uncertainty contribution to the measurement to insignificant levels.

3.2 Edge Recession and Surface Finish

The main metric used in these experiments is edge recession as measured from the plunge cut replications. The initial tool shape of the cutting edge has a nose radius of nominally 500 micrometers. The diamond tools are not a perfect arc; the diamond tip is lapped by a skilled tool maker, and there are some variations in cutting edge sharpness and waviness. The latter translates to a tool with a nose radius that can vary micrometers around the nominal radius. These variations have negligible effect if the nominal tool shape is properly aligned and subtracted from the worn tool profile.

The initial plunge of the “new” tool provides the baseline for the experimental data analysis. A new tool with a uniform edge produces a smooth plunge that can be subtracted from subsequent measurements. The edge-recession extracted from the shape of the plunges in the copper correlates to volumetric diamond tool wear via the tool geometry. With Cu-Ni alloys above the critical level of Nickel the diamond edge used in a test is predicted to recede more than the edge of a tool used in the test of a Cu-Ni alloy below the critical level of Nickel (as described in Chapter 4 section 1). The rate the diamond tool wears varies with the chemical composition of the Cu-Ni, the higher the Nickel content the higher the wear rate, and thus edge recession.

An indirect indicator that the diamond tool is undergoing wear as the cutting distance increases is change in the workpiece surface finish, which is measured at the same intervals as the edge recession measurements are taken. In order to avoid interrupting each test to remove the part several times, the workpiece is diamond turned into a stepped concentric geometry. This removes experimental variability arising from remounting the part and reduces the sensitivity to thermal drift as the entire machining is

process, including plunge cuts, is performed in a single operation with no operator intervention. However, the cutting distance (or time) decreases and average surface speed increases for successive concentric rings

The surface finish of the stepped concentric workpiece areas are measured, typically at 4 places, with a SWLI, the Sq or area RMS (ISO 25178 Part 2) of the surface is plotted versus the cutting distance for each test. Generally, the progression of tool wear leads to degradation of the surface finish. Figure 3.4 below shows schematically the final workpiece, after the test (left) and the white light measurement of a layer (right).

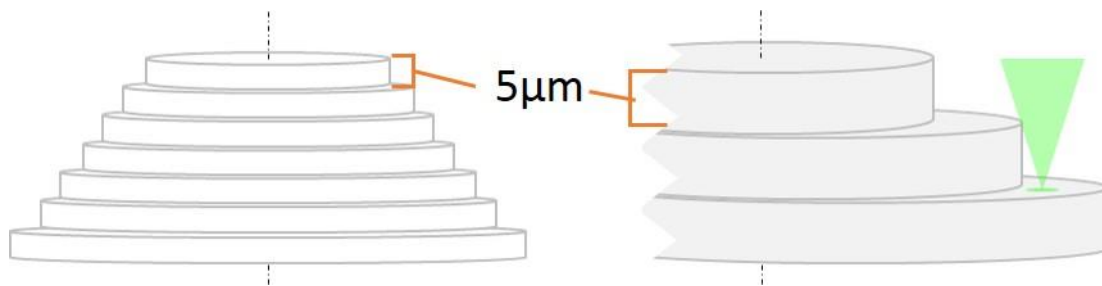


Figure 3.4: The final stepped concentric workpiece after a test (left) with 5 micrometer depths of cut. The measurement of the each step (right) to determine the RMS of the surface at the prescribed cutting distances.

3.3 Metrology Methods and Experimental Setup

The edge recession, which correlates to the diamond tool wear is measured with a witness sample in which the diamond tool edge is replicated. The method used to replicate is to plunge cut the diamond tool into the surface of a plated Oxygen Free High Conductivity (OFHC) Copper ring bolted onto the spindle of the DTM. The plating on the Copper ring is Udylite Bright Acid Copper (UBAC) plated by Epner Technologies in New York with an original thickness of 2 millimeters. The UBAC witness sample is mounted to the spindle with the work piece mounted in the center of the Copper ring,

along the rotational axis of DTM spindle. Figure 3.5 below is an illustration of the witness sample and workpiece mounted to the diamond turning machine from the top view.

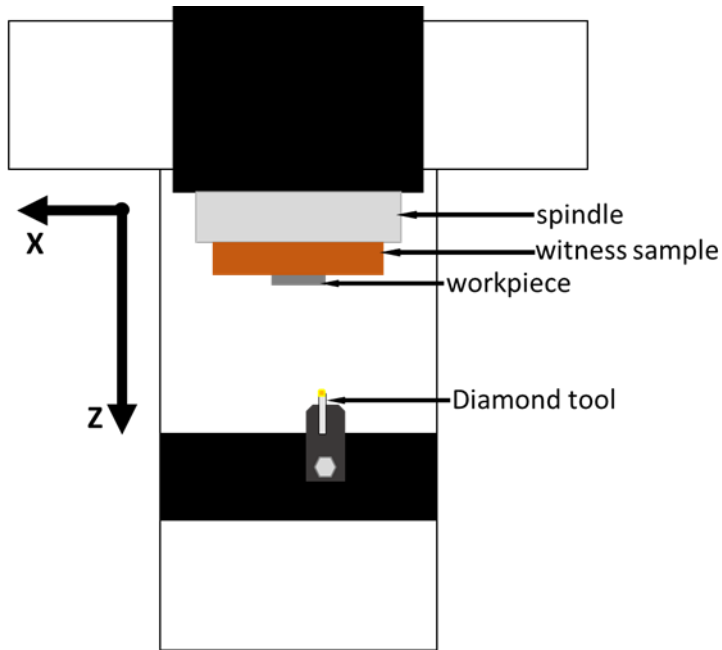


Figure 3.5: An illustration of the top view of the experimental setup used in testing

The surfaces of the witness sample and the workpiece are roughed in, and finished before initiation of the experiment. The theoretical finish of the surface from¹ is 2.5 nm from the well-known equation:

$$h = \frac{f^2}{8R} \quad (3.1)$$

where,

h is the peak-to-valley height of the periodic surface

f is the feed rate in microns per revolution for the testing

R is the radius of the tool tip of the diamond tool

The diamond tools used during the experiments were all fabricated by K&Y Diamond. For the series of tests within this thesis, tools with a nose radius of 500 μ m, a 0° rake angle, and a conical clearance of 6° were chosen, either new tools or ones re-lapped by K&Y were used. Tests were run with 0 degree rotation with respect of the centerline down shank of the tool to minimize diamond orientation effects.

Once the part and ring have been prepared as described above, the surface of the workpiece and the Cu witness sample are touched off (in that order) with a new or re-lapped diamond tool. This establishes the relative coordinate system is for the experiment.

The Precitech diamond turning machine is located in a room with relatively poor temperature control ± 0.5 °C with a limit cycle behavior with a period is approximately 2 hours during typical work days²³. The thermal mass of the large granite base of the machine minimizes the structural loop change during a typical experimental cycle (~65 minutes). However, thermal effects on lower thermal mass components such as the tool post and part mount, as well as spindle growth from start-up are a concern. An example of the thermal effect is found when taking a stylus profilometer trace across the surface of the witness sample (Figure 3.6). After leveling of the profilometer data, the change in plunge cut depth is clearly visible, each plunge is separated by 8 minutes.

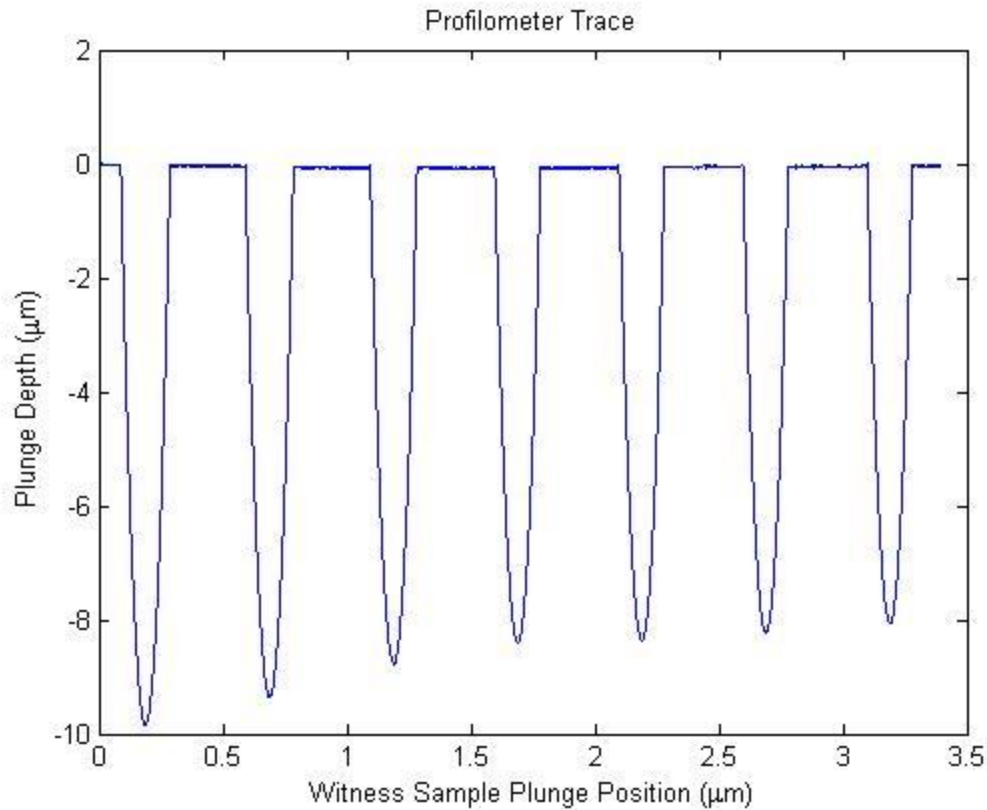


Figure 3.6: A profilometer trace of the UBAC witness sample illustrating the visible change in plunge depth

The acceptance angle of the 20x Mirau objective used for tool wear measurements precludes a plunge cut depth greater than 13 micrometers, the nominal depth of cut is 5 micrometers for all experiments reported here. The data processing method outlined above requires some “unworn” tool on both sides of the center line be included in the plunge cut replica. The protocol used to reduce thermal drift is simply letting the spindle run at the specified speed overnight prior to experimentation, and once the touch off procedure is complete to allow the DTM to thermally soak for an hour.

3.4 Experimental Terminology

Figure 3.7 below is a schematic illustration of the work piece with a stepped concentric geometry. Each band is given a value for k , where $k=1$ is the first band and $k=6$ is the final band removed from the workpiece. The term band refers to the annulus created of material removed, each subsequent band decreases in cutting distance which gives the “wedding cake” look of the workpiece. This allows measurement of the surface finish of the workpiece at the same distances as the plunges are made into the Cu witness sample without interrupting the test in any way.

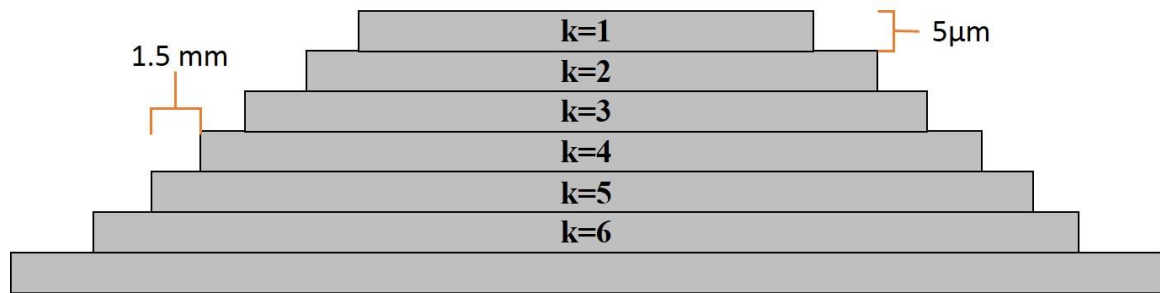


Figure 3.7: A schematic illustration of the stepped concentric workpiece after testing.

Figure 3.8 is an illustrative schematic of the physical variables defining the cutting conditions for the workpiece for the first band of material ($k=1$). The inner radius of the programmed cut (r_k) subtracted from the radius of the uncut workpiece (r_o) leaves the width of the band cut by the diamond tool (l_k). The programmed cutting distance in the controller of the DTM also corresponds to l_k . The depth of cut programmed into the diamond turning machine is C_d . The depth of cut used for all of the bands in the tests run, is 5 micrometers. A general practice in diamond turning is to finish optics with a low (1-5 micrometer) depth of cut, with a feed rate chosen to give low cutting forces and

acceptable finish, for example 2-10 micrometers per revolution of the spindle, depending on the tool nose radius.

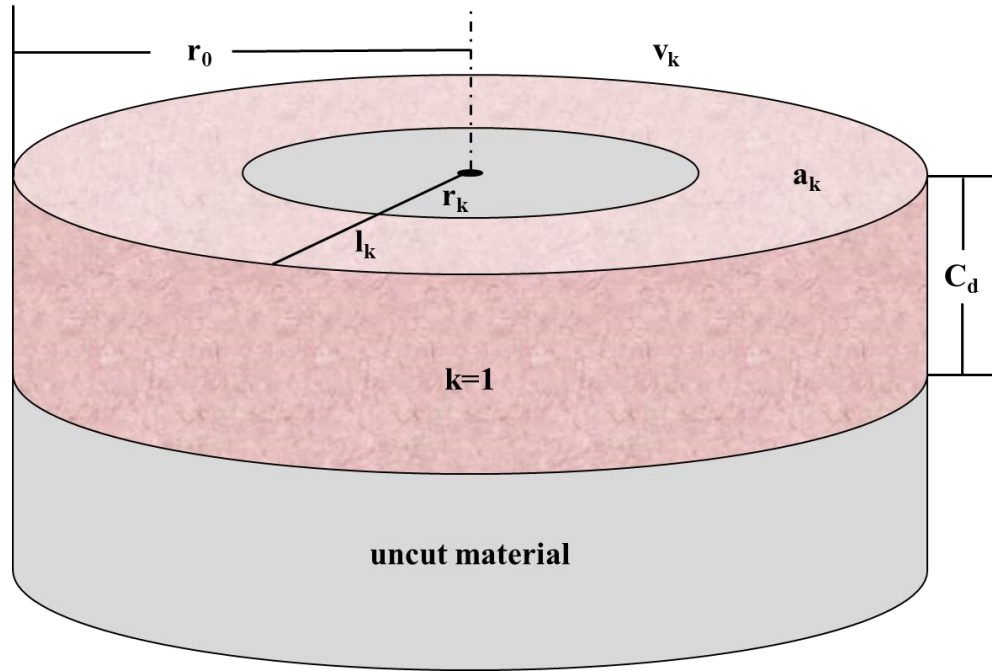


Figure 3.8: A schematic of the annulus removed by the diamond tool, and the variables associated with each band.

In the diamond turning literature, it is common to describe the effect of tool wear (for example change in surface finish) as a function of cut distance, which seems natural to the tribologist (T. Childs). In the case of chemical wear it is not clear that this is the best metric. The theoretical chemist on the project (E. Paul) naturally gravitates to volume removed. The presumption that the mechanism is a surface reaction suggests that contact time be considered.

The area of the top surface of the band removed from the workpiece is a_k from:

$$a_k = \pi(r_0^2 - r_k^2) \quad (3.2)$$

where,

r_0 is the outer radius of the band on the workpiece

r_k is the inner radius of the band on the workpiece

a_k multiplied by the depth of cut in millimeters is the volume of the band v_k removed by diamond turning for each k value, given by the equation:

$$v_k = C_d * a_k \quad (3.3)$$

The cutting time of each layer is given when the band width l_k is divided by the feedrate (f) in millimeters per minute. The federate in micrometers a revolution (f^*) is the feedrate f , divided by the angular velocity of the spindle (Ω). In diamond turning, a common metric for how much use a diamond tool has undergone is the cutting distance. In each of the bands cut the cutting distance per band is given by equation 3.4 below:

$$d_k = \pi(r_o^2 - r_k^2) \frac{\Omega}{f} = \frac{a_k \Omega}{f} = \frac{a_k}{f^*} \quad (3.4)$$

where,

d_k is cutting distance of the diamond tool on the workpiece in meters

f is federate of the diamond tool in millimeters per minute

f^* is federate of the diamond tool in micrometers per revolution

Ω is the angular velocity of the spindle in rotations per minute

The average velocity per band increases as the bands have a smaller l_k value as the experiment progresses. The average velocity per band $\langle v_k \rangle$ is given by equation 3.5 below:

$$\langle v_k \rangle = \frac{d_k}{t_k} \quad (3.5)$$

where,

d_k is cutting distance of the diamond tool on the workpiece in meters

t_k is cutting time of each band in minutes

Table 3.1 below shows terminology.

Table 3.1: Variables used to describe the parameters selected during the testing of chemical diamond tool wear

Variable	Equation	Description	Units
k	N/A	The identifier of each band	N/A
r_o	N/A	Radius of uncut workpiece	mm
r_k	N/A	The inner radius of band k	mm
C_d	N/A	Depth of cut for the diamond tool	μm
l_k	$r_o - r_k$	Width of diamond turned band k	mm
a_k	$\pi(r_o^2 - r_k^2)$	Area of the top surface of band k	mm^2
v_k	$C_d * a_k$	Volume of the band k	mm^3
Ω	N/A	Angular velocity of the Spindle	RPM
f	N/A	Feedrate of the diamond tool	mm/min
f^*	f/Ω	Feedrate of the diamond tool	$\mu\text{m}/\text{rev}$
d_k	$a_k \Omega / f = a_k / f^*$	The cutting distance of band k	m
t_k	l_k / f	Time to cut band k	minutes
$\langle v_k \rangle$	d_k / t_k	Integral average velocity of band k	m/s

3.5 Experimental Parameters and Conditions

The initial approach was to test the theory that Cu-Ni alloys with 33 wt% Ni or a d-index of 10 (Chapter 4, section 2) or higher would give chemical wear on diamond tools, and below this critical percentage or d-index chemical diamond tool wear would not occur. In order to verify this an initial test of three materials Monel (all references to Monel in this thesis are to Monel 400, Cu 32 Ni 62 wt%), Cu 70 Ni 30wt% alloy, and a Cu 90 Ni 10 wt% alloy; was conducted. Samples were prepared with a nominal r_o of 20 millimeters, and the initial parameters chosen are shown in Table 3.2. The initial l_k value is 19.5 millimeters and decreases 3 millimeters per band until $k=6$ and the experiment is complete. Cutting distance per band decreases from d_1 to d_6 , while the average velocity,

$\langle v_k \rangle$ increases per band. The diamond tools used were all new or newly re-lapped tools, and the set normal to the workpiece for this set of testing.

Table 3.2: The parameter space for the initial set of tests in order to test the d-index theory.

Depth of Cut (mm)	0.005	Run				Long		
Depth of Cut (μm)	5	Angular Velocity (RPM)				1000		
Tool Radius (mm)	0.5	Feedrate (mm/min)				2		
clearance angle ($^\circ$)	6	Feedrate (mm/revolution)				0.002		
k	$r_0(\text{mm})$	$r_k(\text{mm})$	$l_k(\text{mm})$	$a(\text{mm}^2)$	$v(\text{mm}^3)$	$d_k(\text{m})$	$t_k(\text{minutes})$	$\langle v_k \rangle (\text{m/s})$
1	19.9	0.4	19.5	1243.60	6.22	621.8	9.75	1.06
2	19.9	3.4	16.5	1207.79	6.04	603.9	8.25	1.22
3	19.9	6.4	13.5	1115.42	5.58	557.7	6.75	1.38
4	19.9	9.4	10.5	966.51	4.83	483.3	5.25	1.53
5	19.9	12.4	7.5	761.05	3.81	380.5	3.75	1.69
6	19.9	15.4	4.5	499.04	2.50	249.5	2.25	1.85

The final stepped concentric workpiece resembled figure 3.6, where the first value l_1 is 19.5 millimeters and decreasing 3 millimeters each band to where l_6 is 4.5 millimeters. These conditions have significant tool wear on the Monel (see Chapter 4 for more details) A second set of cutting conditions (Table 3.3, referred to as a “short run”), decreased the l_k values by 10 millimeters for the first band and reducing Δl_k from 3mm to 1.5 mm. The shorter cutting distances increased the resolution of the effects of the wear on the diamond tools.

Table 3.3: The parameter space for the short run tests to increase the resolution of the wear in the diamond tool.

Depth of Cut (mm)		0.005	Run			Short		
Depth of Cut (μm)		5	Angular Velocity (RPM)			1000		
Tool Radius (mm)		0.5	Feedrate (mm/min)			2		
clearance angle ($^\circ$)		6	Feedrate (mm/revolution)			0.002		
k	$r_o(\text{mm})$	$r_k(\text{mm})$	$l_k(\text{mm})$	$a(\text{mm}^2)$	$v(\text{mm}^3)$	$d_k(\text{m})$	$t_k(\text{minutes})$	$\langle v_k \rangle (\text{m/s})$
1	19.9	10.4	9.5	904.31	4.52	452.2	4.75	1.59
2	19.9	11.9	8	799.22	4.00	399.6	4.00	1.67
3	19.9	13.4	6.5	680.00	3.40	340.0	3.25	1.74
4	19.9	14.9	5	546.64	2.73	273.3	2.50	1.82
5	19.9	16.4	3.5	399.14	2.00	199.6	1.75	1.90
6	19.9	17.9	2	237.50	1.19	118.8	1.00	1.98

Results obtained from plunge cuts into OFHC copper were occasionally confounded by obvious “chips” which were attributed to hard inclusions in the copper. The OFHC copper ring was plated on the plunge cuts into the witness sample, and had the witness sample plated with UBAC. No further chipping was observed.

The theory of the chemical diamond tool wear Paul et al.⁶ suggested a strong dependence on the thermal effects of the diamond workpiece interface. Series of experiments systematically vary surface speed (Table 3.4), feedrate (Table 3.5), and contact time (Table 3.6).

Table 3.4: The parameters under test for the variation of surface speed testing, which also varies the cutting time.

Test 1			Test 2			Test 3		
500			1000			2000		
1			2			4		
0.002			0.002			0.002		
$d_k(m)$	$t_k(minutes)$	$\langle v_k \rangle (m/s)$	$d_k(m)$	$t_k(minutes)$	$\langle v_k \rangle (m/s)$	$d_k(m)$	$t_k(minutes)$	$\langle v_k \rangle (m/s)$
452.2	9.50	0.79	452.2	4.75	1.59	452.2	2.38	3.17
399.6	8.00	0.83	399.6	4.00	1.67	399.6	2.00	3.33
340.0	6.50	0.87	340.0	3.25	1.74	340.0	1.63	3.49
273.3	5.00	0.91	273.3	2.50	1.82	273.3	1.25	3.64
199.6	3.50	0.95	199.6	1.75	1.90	199.6	0.88	3.80
118.8	2.00	0.99	118.8	1.00	1.98	118.8	0.50	3.96

Table 3.5: Testing holding the surface speed and varying the feedrate during turning Monel.

Test 1			Test 2			Test 3		
1000			1000			1000		
5			10			15		
0.005			0.01			0.015		
$d_k(m)$	$(minute)$	$\langle v_k \rangle (m/s)$	$d_k(m)$	$t_k(minutes)$	$\langle v_k \rangle (m/s)$	$d_k(m)$	$t_k(minutes)$	$\langle v_k \rangle (m/s)$
180.9	1.90	1.59	90.4	0.95	1.59	60.3	0.63	1.59
159.8	1.60	1.67	79.9	0.80	1.67	53.3	0.53	1.67
136.0	1.30	1.74	68.0	0.65	1.74	45.3	0.43	1.74
109.3	1.00	1.82	54.7	0.50	1.82	36.4	0.33	1.82
79.8	0.70	1.90	39.9	0.35	1.90	26.6	0.23	1.90
47.5	0.40	1.98	23.8	0.20	1.98	15.8	0.13	1.98

Table 3.6: The tests holding the feedrate constant while varying the surface speed on Monel.

Test 1			Test 2			Test 3		
500			1000			2000		
2			2			2		
0.004			0.002			0.001		
$d_k(m)$	$t_k(minutes)$	$\langle v_k \rangle (m/s)$	$d_k(m)$	$t_k(minutes)$	$\langle v_k \rangle (m/s)$	$d_k(m)$	$t_k(minutes)$	$\langle v_k \rangle (m/s)$
226.1	4.75	0.79	452.2	4.75	1.59	904.3	4.75	3.17
199.8	4.00	0.83	399.6	4.00	1.67	799.2	4.00	3.33
170.0	3.25	0.87	340.0	3.25	1.74	680.0	3.25	3.49
136.7	2.50	0.91	273.3	2.50	1.82	546.6	2.50	3.64
99.8	1.75	0.95	199.6	1.75	1.90	399.1	1.75	3.80
59.4	1.00	0.99	118.8	1.00	1.98	237.5	1.00	3.96

3.6 Direct and Indirect Tool Wear Metrology

The concentric stepped workpiece and the UBAC witness sample after testing are removed from the diamond turning machine. The samples are drag-wiped to remove excess debris from the surface and prepared for metrology. Most measurements are taken using the 20x objective is placed on the ZeGage SWLI. The field of view of the 20x objective is 417 x 417 micrometer square on a 1024x1024 detector, giving a pixel size in object space of 407 nm, giving a Nyquist limit of 0.81 microns. This is a reasonable match to the optical resolution, R , given by the Rayleigh criterion:

$$R = \frac{\lambda}{2NA} \approx \frac{0.55}{2(0.4)} \approx 0.7 \mu\text{m}$$

where, λ is the center wavelength of the green illumination and the objective numerical aperture (NA) is 0.4. In order to resolve finer structure, some measurement were made with the 50x objective (NA=0.55), giving an optics limited resolution of 0.5 μm .

The workpiece roughness is measured at four locations on each band. Figure 3.9 shows a typical plot of area RMS, Sq (ISO 25178-2) against the cutting distance in km. This provides a functional, indirect measure of tool wear which affects both the fine structure of the surface and increases the cutting force, leading to dynamic effects and grain relief.

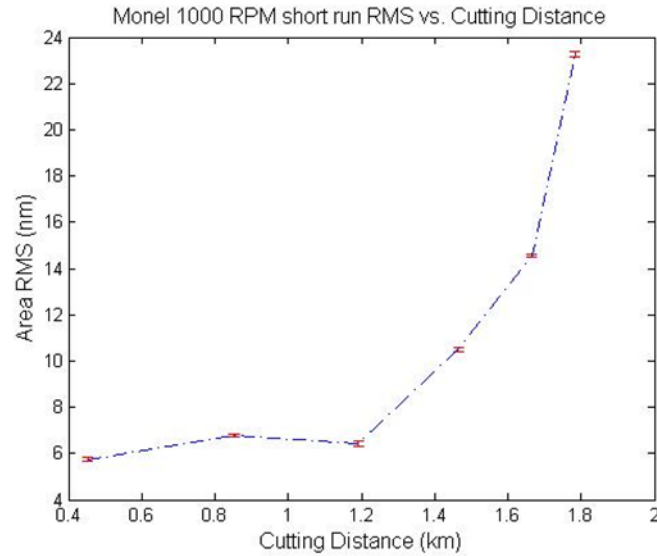


Figure 3.9: The Area RMS (Sq) of the stepped concentric workpiece plotted versus the Cutting distance.

The witness sample is also measured on the ZeGage; each plunge cut replication is measured, using an average of four scans at four locations per plunge cut. The raw data from the interferometer provides useful information, but must be processed to provide quantitative edge recession data as a function of position around the tool, i.e. the direct tool wear data. This data will be used to compare with predicted local temperature (FEA and analytical, Childs) and to calculate activation energies (Paul). The final output is the change of the shape of the diamond tool, referred to in this thesis as a “residual”, or the total diamond tool wear obtained by subtracting to unused tool profile from each replication in the UBAC witness sample at the different cutting distances. Note that the removal per pass (or layer) can also be computed. The secondary output, or indirect measurement is the surface finish data, discussed above.

In order to calculate the residuals, the raw data acquired by the SWLI is processed in Matlab. The raw data is converted from the Zygo proprietary file format .dat to a

Matlab .mat file, which represents the height map of the surface measured. Figure 3.10 is the Raw data from the ZeGage (left) and the conversion to the Matlab variable (right).

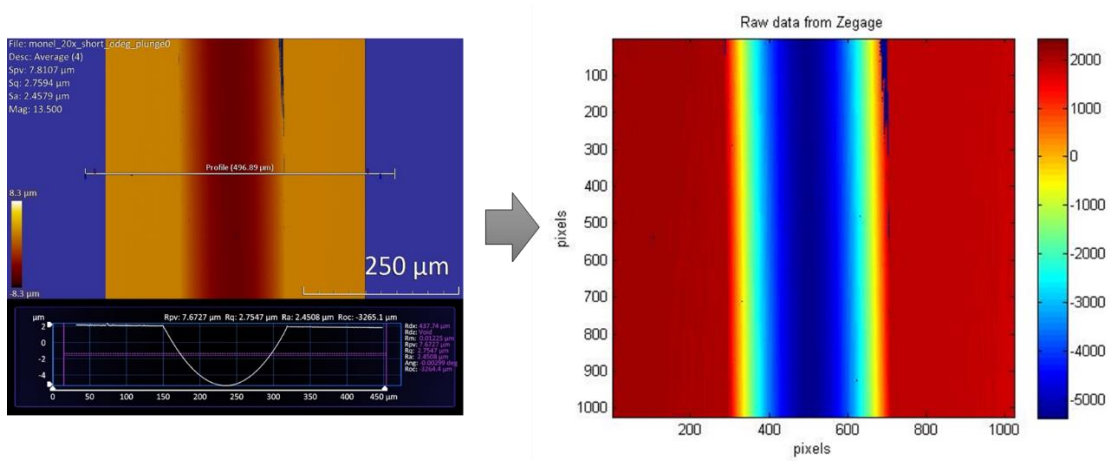


Figure 3.10: The raw data from the ZeGage™ in .dat form (left) converted to the Matlab variable as a three dimensional matrix of points (right).

In previous work, Griffin¹⁶ fitted the plunge data to a cylinder, representing the nominal tool shape. Here the data are converted to an average profile by averaging “columns”. Hence the vertical alignment of the height map is important, (the height map) is rotated based on the transition between the uncut plane (left and right of Figure 3.11) and the plunge. Figure 3.11 shows the raw data in Matlab before rotation (left) and the rotated data (right).

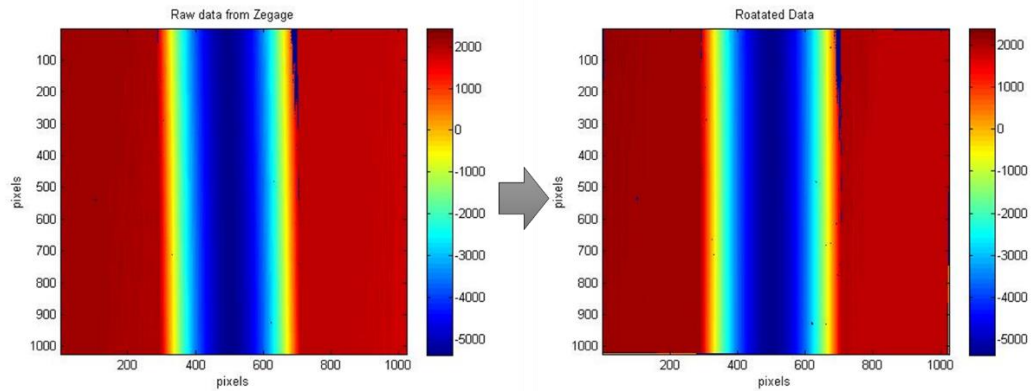


Figure 3.11: The raw plunge data (left) is rotated, aligning the plunges for subsequent steps (left.)

During the measurement of the plunge the fringes are nulled, removing the majority of the tilt. The remaining tilt in the measurement of the plunge is removed by fitting a plane to the flats on both sides of the plunge and subtracting it from the rotated plunge. In Figure 3.12 below the rotated data (left) is tilt-corrected (right).

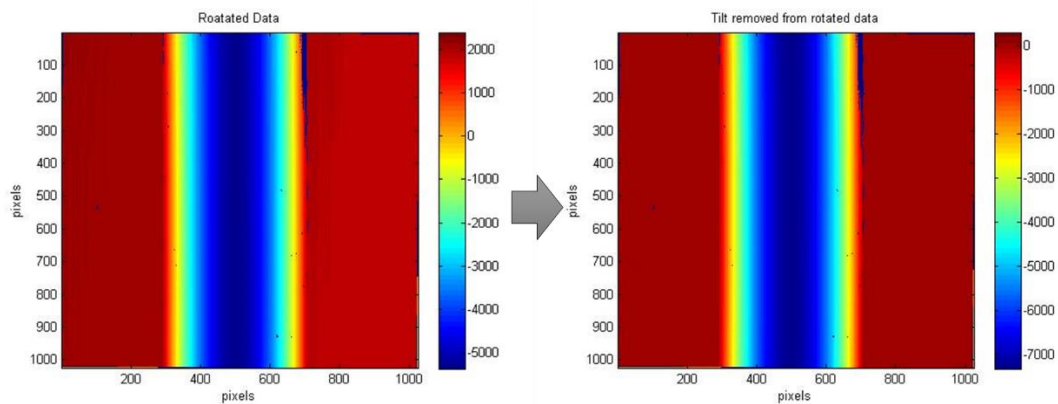


Figure 3.12: The rotated data (left) is tilt corrected (right) by fitting a plane to the flats and subtracting it.

The flats, which are useful in the rotation and tilt correction of the plunge, are no longer of use and are removed from the height map, leaving the plunge. To this point, the processing for one plunge has been explained. In order to subtract the initial tool shape

from the subsequent plunges they must all be aligned and centered about zero. Rather than process matrices, the columns are averaged to create a profile in which electronics noise and other sources of time varying uncertainty are minimized. The averaged profile of the plunge is then centered to zero, with the leading edge of the diamond tool being the negative values. Initial centering of the plunge uses the unworn section of the plunge “above” the nominal depth of cut and finding an average vector point-by-point that identifies the center of the tool. Figure 3.13 shows the rotation and tilt corrected plunge (top left), the flats removed (top right), un-centered plunge (bottom left) and the centered plunge (right). The remaining centered plunge will be used to calculate the residual diamond tool wear.

The process above for a single plunge is completed for the initial unworn tool replication and the six subsequent plunges, where they are all plotted together. Once they are all plotted together and subtracted there is an issue with alignment. If the plunges are not aligned properly there is a positive or negative slope biasing the data. The most significant reason for alignment issues is the sub-pixel alignment errors. In order to resolve the alignment errors a linear interpolation of 100 data points between each data point was processed, and based on a tilt sensitivity which is degrees of shift per sub pixel shift the angle is corrected by shifting the plunges 1-6 positively or negatively based on the slope of the unworn tool on the trailing edge of the diamond. In the below series of

figures the unworn tool and the final plunge of the Monel short experiment with experimental parameters found in Table 3.3.

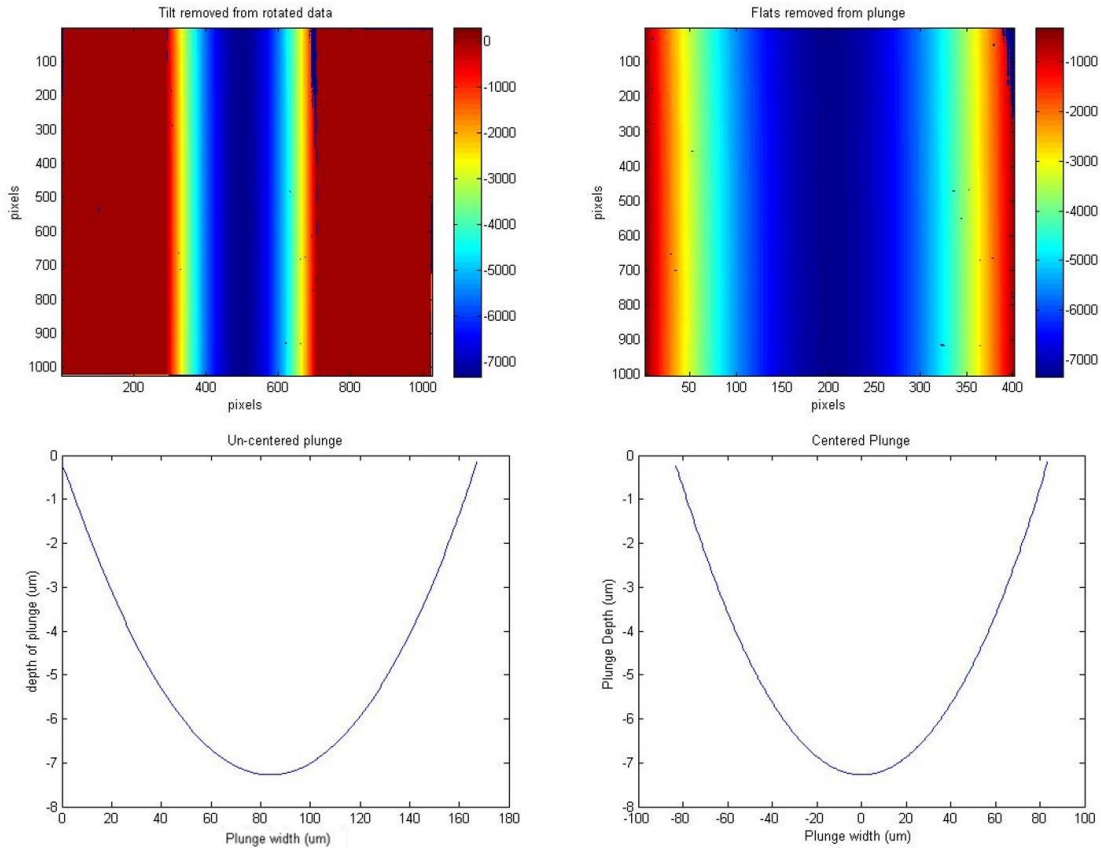


Figure 3.13: The rotation and tilt corrected image, (top left) the same plunge with the flats removed. (top right) The plunge is averaged down the columns creating an average profile of 1024 rows, un-centered (bottom left). The plunge is then centered about zero by using the uncut area of the plunge (bottom right).

The first figure, Figure 3.14 below, is the initial plunge of an experiment which is a replication of the unworn diamond tool, and the final plunge plotted together, the left limit of data and right limit are selected and the initial plunge is subtracted from the final plunge. Once the initial tool shape is subtracted from the final plunge a residual of the worn diamond remains with an angle derived from the misaligned subtraction of two quadratics. The angular shift θ per sub-pixel being known, the angle of the unworn

section of the trailing edge of the diamond tool is found by fitting a line. Figure 3.15 shows the initial subtraction of the two quadratics.

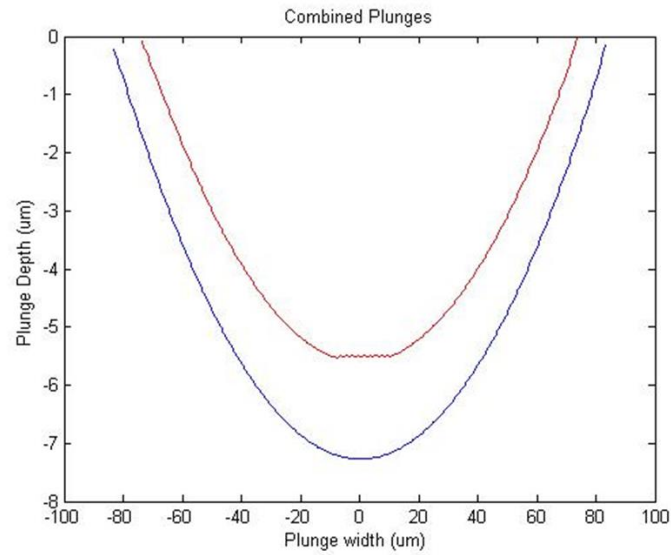


Figure 3.14: The replication of the unworn tool and the final plunge for the diamond tool wear experiment for selection of the left and right limits, and subsequent subtraction of the initial tool shape from the final plunge.

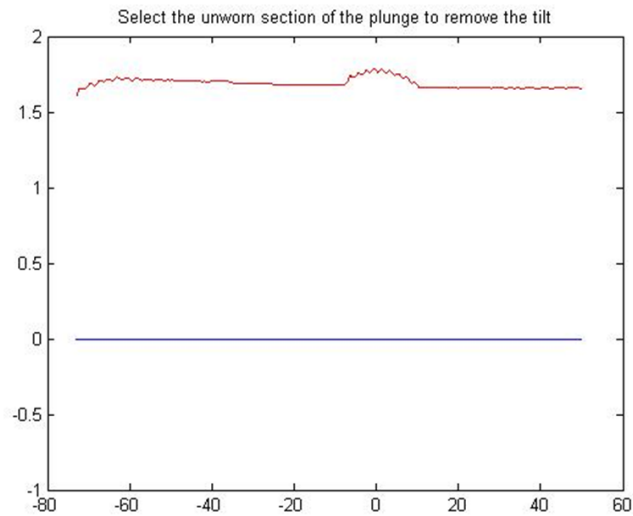


Figure 3.15: The residual of the subtraction of the two plunges, the initial plunge (bottom) and the final plunge (top)

After the unworn section on the right is subtracted, the vector is shifted either in a positive or negative direction. The shifted data; based on the unworn section of the trailing edge of the diamond tool, is then corrected for the DC offset from the SWLI. Figure 3.16 shows the final residual of the initial plunge and the final plunge. The process in this section is meant solely to demonstrate the process, the data processing for each experiment completes this for each plunge giving combined residuals of each plunge.

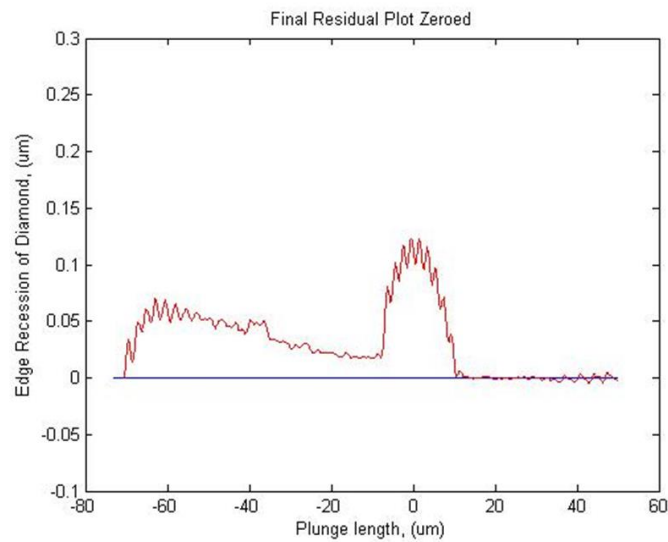


Figure 3.16: The final aligned residual of the initial plunge and the final plunge after tilt correction

CHAPTER 4: MATERIAL CONSIDERATIONS

In their National Science Foundation (NSF) proposal, Evans and Paul¹⁴ suggested that the chemical wear of a diamond tool in machining a single phased alloy might be related to alloy composition via an effective number of d-shell electrons, assuming the formation of an energy level combining d and s or p shell electrons. Conceptually, the wear rate, measured using the methods described in Chapter 3, should be related to the composition for a chemical wear mechanism.

In Paul et al.⁶ they made this argument, conceptually, for the Ni-P system. This thesis considers the Cu-Ni system, for which there is little published diamond wear data, although there are indications of successful single crystal diamond machining “nickel silver”²⁴. The equilibrium phase diagram for the copper – nickel alloy system (Figure 4.1) shows single phased alloys at all compositions.

Historically¹, copper is considered “diamond turnable” and pure nickel is not. Copper has no unpaired d-shell electrons (the d-shell is full) and nickel has 2 (i.e. 8 d-shell electrons). At high copper concentrations in a Cu-Ni alloy, the Cu s-shell electrons may effectively “fill” the d-shell of the nickel (to the extent that the shell model is an appropriate descriptor). Commercially available Cu-Ni alloys all contain some iron and manganese, both of which have unpaired d-shell electrons. Estimates of the d-index must take these trace amounts into consideration.

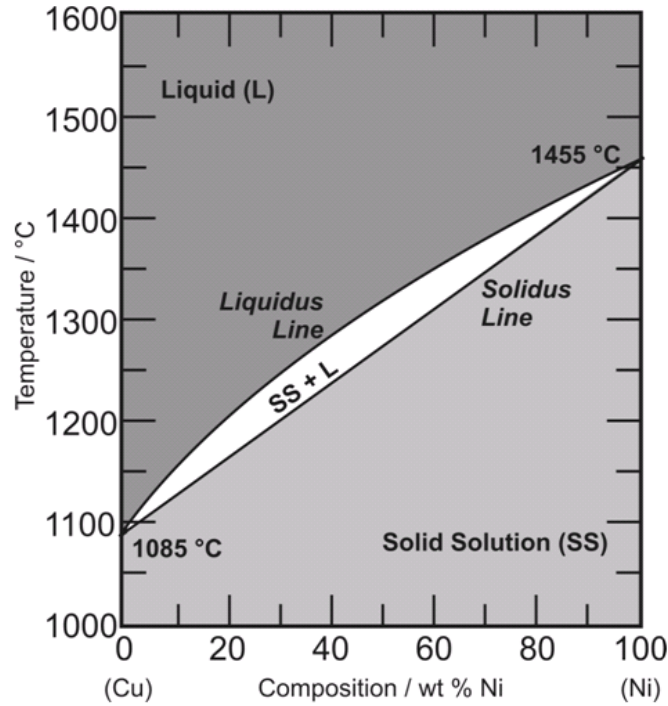


Figure 4.1 Cu-Ni Phase diagram showing the solid solution of across the range of compositions⁷.

4.1 Effective D-index

The theory behind calculating the d-index is described in the NSF proposal¹⁴, for commercially available alloys, the composition of each alloy, in Cu, Ni, Mn, and Fe has a defined range, giving an uncertainty in the d-index. Some of the alloys used in this research were provided with certified compositions. This reduces the uncertainty in d-index calculations.

The derivation of the d-index begins with known composition and molar mass (MW) of each element present in the alloy. Equation 1 shows how to calculate the mol per element (n) in the alloy

$$\frac{wt\%_n}{MW\%_n} = mol_n \quad (1)$$

Then in order to calculate the molar fraction (mf_n) of each element:

$$\frac{mol_n}{mol_{total}} = mf_n \quad (2)$$

Using mf_n and the d electrons $n_{d_{e-}}$ in each element as well as the added (e.g. s-or p shell) electrons $a_{d_{e-}}$.

$$d_n = mf_n * (n_{d_{e-}} + a_{d_{e-}}) \quad (3)$$

Where d_n is the total d electrons per element, then summing all of d_n for each alloy we arrive at the equation to calculate the effective d-index.

$$d_{eff} = d_{Cu} + d_{Ni} + d_{Mn} + d_{Fe} \quad (4)$$

Table 4.1 shows the d-index for materials machined in this work. Copper, with a full d-shell and one s-shell electron has a d-index = 10+1.

4.2 Materials of interest

The materials chosen for testing are all commercially available Table 4.1 below tabulates the alloys by composition and decreasing effective d-index using the certified compositions (where available) for the alloys purchased. The nickel was specified as 99.999% purity, although no certification was provided. The constantan and British 10 pence coin values are nominal.

Table 4.1: The tested alloys by nominal composition from manufacture certifications, and the nominal effective d-index.

	Nominal Values				
Alloy	Cu (wt%)	Ni (wt%)	Mn (wt%)	Fe (wt%)	d-index
Cu	100.0	0.0	0.0	0.0	11.000
90/10	87.3	10.4	0.7	1.7	10.526
10 Pence	75.0	25.0	0.0	0.0	10.204
70/30	67.5	31.1	0.7	0.7	9.931
Constantan	55.0	45.0	0.0	0.0	9.591
Monel	32.5	64.6	1.0	1.9	8.850
Ni	0.0	100.0	0.0	0.0	8.000

Nickel has the lowest d-index, and is predicted to give the highest chemical wear. Quantitative measurements of that wear provide a direct link to the qualitative observations of Paul et al⁶. Monel, a sea water resistant Ni-Cu alloy used in chemical, oil and marine applications; with a d-index below 9, it is expected to cause significant chemical wear. Note, that the chemical wear is expected to be a function of both the composition of the material and the local temperature at the tool-workpiece interfaces. Hence the materials properties of the sample and history of the sample (prior work hardening, for example) is expected to affect chemical wear rates. Complementary research to the work reported here is underway to predict local temperatures and cutting forces.

Constantan, also known as Eureka, is expected to have some chemical wear effects on the diamond tools. Note the similarity to the 70/30 alloy the next highest d-indexed material. The d-index values above are similar even though the Nickel contents are not. This is due to the trace Mn and Fe in the 70/30 which are not present in the Constantan. Mechanically the two alloys are quite different, with the Vickers hardness of the Constantan ranging from HV 100 to 316, and annealed 70/30 a HV of 95.

The Ten Pence (10p) British coin is a Cu-Ni alloy without any trace elements reported in the open literature. EDAX measurements, however, showed, a Ni composition of approximately 35wt %. As Childs points out (personal communication, 2014) it is unlikely that the British mint debased the coinage by increasing the content of the more expensive component (Ni). At higher Ni contents, the surface oxide of Cu Ni alloys is preferentially nickel oxides, which may skew the EDAX result. The EDAX also

showed >1% Mo, which will affect the d-index. The lowest Ni content alloy; 90/10, tested contains trace elements of Mn and Fe.

The range of d-index values for materials machined in these studies varies from 11.0 for pure copper which is chemically inactive with diamond tools to 8.0 for pure nickel, previously shown to rapidly wear diamond tools. The addition of manganese and iron within the alloys causes the variations in the d-index. The hypothesis advanced by Evans and Paul¹⁴ is that the critical d-index value is 10 or Ni 33 wt% in the alloy composition of the Cu-Ni with no trace impurities with unpaired d-shell electrons. Local temperature will influence the observed wear. Figure 4.2 shows the d-index as a function of nickel content for pure Cu-Ni alloys.

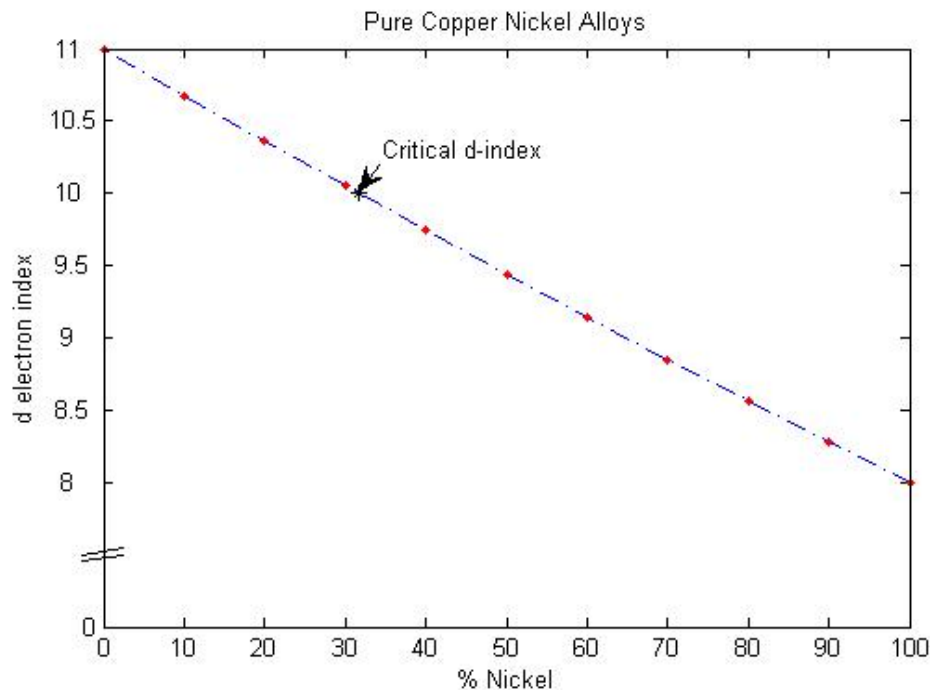


Figure 4.2: The d-electron index versus the Ni wt%, when the Ni content corresponds with a d-index value of 10 or lower the chemical wear is predicted.

CHAPTER 5: RESULTS AND DISCUSSION

A series of facing tests on a set of Cu-Ni samples (Chapter 4) were performed using the test procedures described in Chapter 3. Using the interferometric measurement of plunge cuts (also described in Chapter 3) a variety of different diamond tool wear mechanisms were observed. These include nose flattening, chipping, Pecalharing grooves, propagation of tool defects, and finally chemical wear of diamond tools.

5.1 Copper Witness Sample

Initially OFHC copper was selected as the witness sample. It has been widely used for water cooled IR laser mirrors and is generally considered “diamond turnable”. Shimada²⁵ showed cutting distances of 70 km with negligible diamond tool wear. Impurities in OFHC copper may, however, lead to abrasive wear and chipping of the tool edge. Figure 5.1 shows the measured wear cutting Cu70Ni30 (short run conditions in Table 3.3). Zero on the abscissa represents the position of the nose of the unworn tool. The leading edge (from nose to the depth of cut line) where cutting nominally takes place, is represented by negative values of plunge position. In the absence of wear at the nose, the trailing edge (positive values) only cuts during the plunge replication process.

Note in Figure 5.1 the wear centered at approximately 35 μm . It appears that a chip was introduced into the trailing edge during the plunge cut after the first pass across the sample (Residual 1). There is no subsequent change in this area over the rest of the test cycle. The leading edge, specifically in the range from -25 to -60 μm shows “break

in” wear followed by little change in the tool profile. In addition there is ~50 nm of nose wear in the first pass, followed by a slow evolution through the 4th pass (residual 4). During the 5th pass (or the plunge cut) a further chip (plunge positions between -10 and -20 μm) appears in the leading edge, and is essentially unchanged in the 6th pass. It is not possible to determine if this occurs during machining of the sample or during the plunge cut.

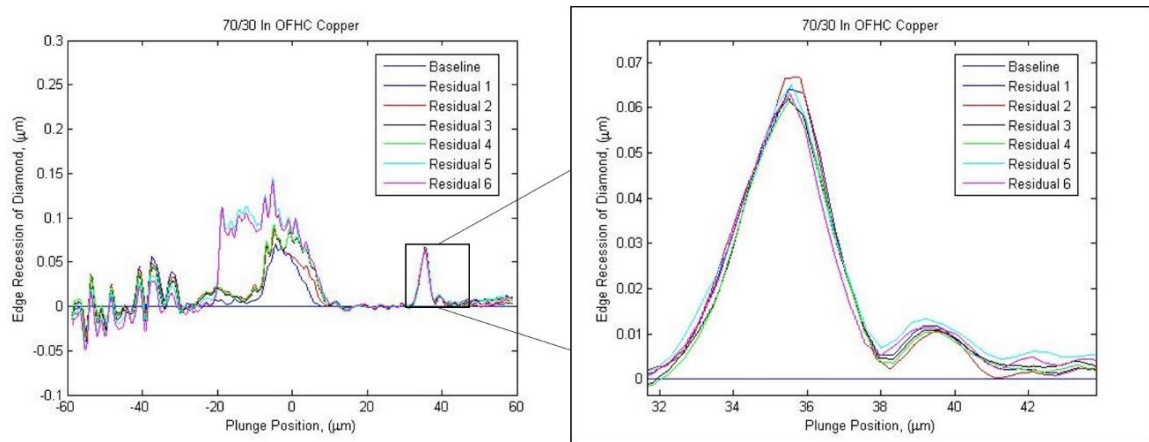


Figure 5.1: The OFHC copper ring caused pieces of diamond to be knocked out on the trailing edge during testing.

The cause for the diamond tool to chip in the trailing edge must be from inclusions or hard particles in the OFHC witness sample or an edge defect in the tool. Copper has been used as a witness sample for tool qualification¹⁸ and tool wear measurement in diamond turning⁵, and low ductility copper plating has been used in industry for plating diamond turned rolls used to produce high brightness retro-reflective films²⁶. Udylite Bright Acid Copper (UBAC) is a fine grained, low ductility copper plating that has been used in critical diamond turning application over 20 years or so. Figure 5.2 shows the wear resulting from 7 cycles of plunge cutting into a UBAC

witness. These results show negligible tool wear contributions from the UBAC witness sample (less than 10 nm), the left figure on the same scale as the other residuals and the right, the vertical scale in nanometers.

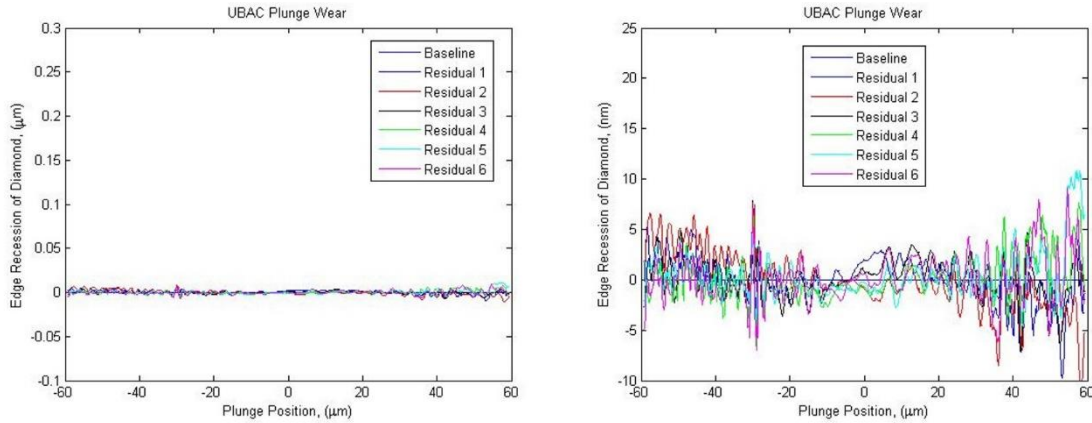


Figure 5.2: Duplication of replication process in the diamond tool wear testing in the Cu witness sample. The Left figure on the same scale as other residual plots, and the right with a smaller vertical scale (nm).

5.2 Diamond Tool Wear Categories

The most prevalent form of wear observed is nose flattening. This occurs over a limited range of chip thickness where, presumably, there is significant elastic and plastic deformation. This resulting temperature rise will locally accelerate chemical wear (Figure 5.3). The apparent rounding in this area arises because the “residual” is a measure of the material removed, not the tool shape.

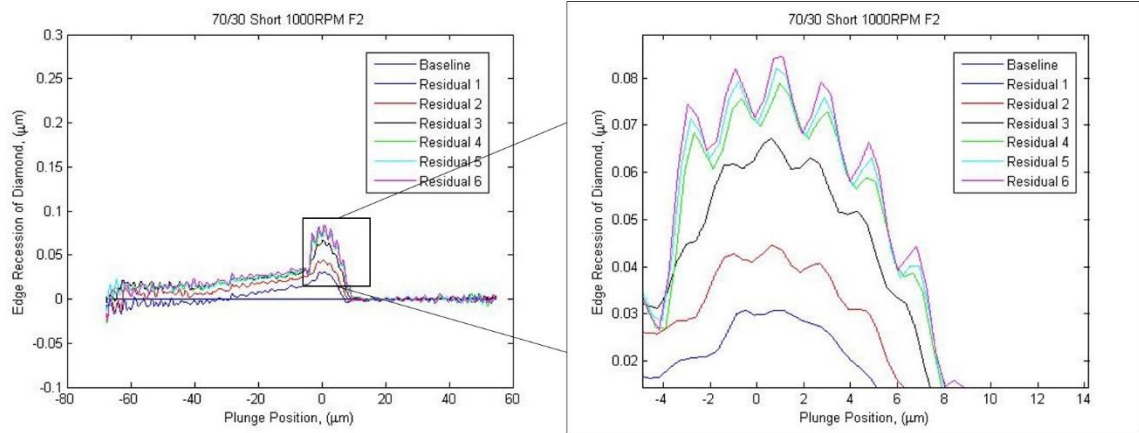


Figure 5.3: The edge recession of the diamond tool nose gives proof that as the cutting distance and time increase the diamond tool wear also increases.

The higher frequency grooves on the edge of the diamond tool appear to be Pecalharing grooves which occur at the feedrate of cut in conventional tooling. The mechanisms for groove formation are discussed, for conventional tool materials, by Pecalharing²⁷. The grooves in the diamond tools are observed in many of the experiments performed, and occur at the feedrate ($2\mu\text{m}/\text{rev}$ in this case). Figure 5.4 shows the filtered data of the sixth residual in Figure 5.3, after passing through a high pass filter with a $4\mu\text{m}$ cutoff. The period of the grooves is the same as the feedrate. The mechanisms described by Pecalharing do not seem reasonable for diamond wear; further study is required.

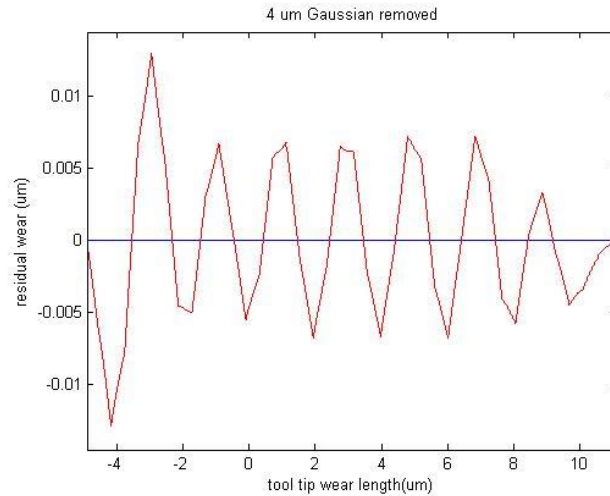


Figure 5.4: The Pekalhari grooves with a 2 μm period in the diamond tools, through a high pass filter with a 4 μm cutoff (0.41 $\mu\text{m}/\text{pixel}$).

The leading edge of the diamond tool removes material with a varying chip thickness, and hence presumably local temperature. As the nickel content of a Cu-Ni alloy increases, the d-index decreases, and thus the leading edge chemical wear is expected to increase. Figure 5.5 shows wear of Cu70Ni30 an alloy expected to hover around the critical d-index value of 10 (Chapter 4); there is some edge recession, but the amount is small compared to the edge recession of the Monel (right) which has a lower d-index.

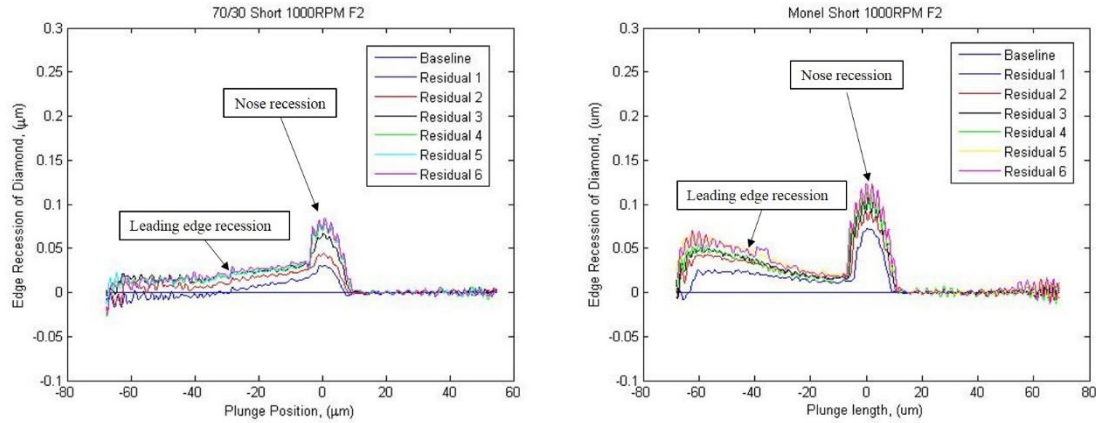


Figure 5.5: Cu70Ni30 (left) an alloy expected to hover around the critical d-index value of 10, has some edge recession, but a lower amount than the edge recession of the Monel (right) which has a lower d-index and thus more leading edge chemical wear.

When there are defects in the diamond tool, for example from lapping or errors in touch off, the interferometric method can detect the faster propagation, perhaps along a crystallographic plane or a local defect in the diamond. The reasoning for that assumption is in Figure 5.6, where the edge-recession has a trend which is not normal to the local tool-workpiece contact. In addition SWLI measurements of the rake surfaces of these tools show linear discontinuities. The figure on the left is the residuals of the tool wear, on the right is with a fit quadratic of the unworn tool added in, to show the trend on the tool tip.

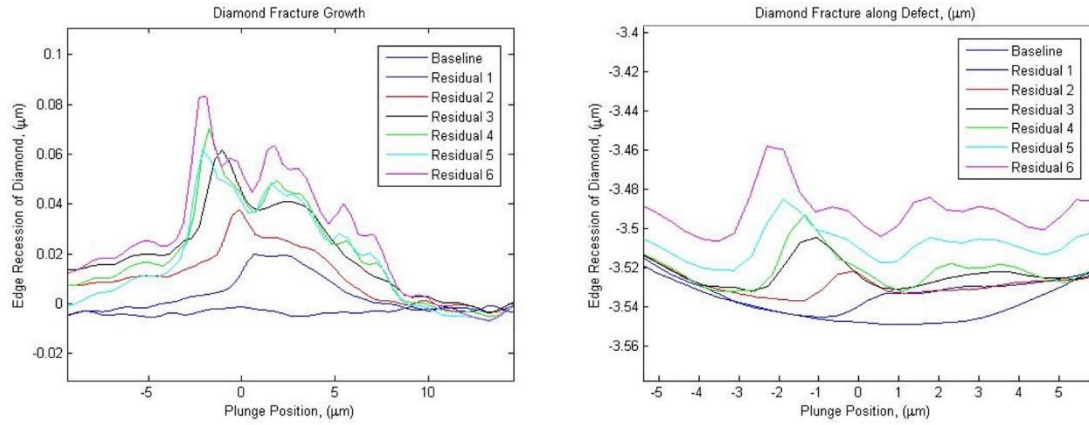


Figure 5.6: The residuals with a fit quadratic removed from the unworn tool (left), and the same quadratic added into the residuals to show the propagation of the defect.

5.3 Alloys of Varying Composition

The following figures are the residuals for the set of tests which tested the diamond tool wear under similar conditions, outlined in Chapter 3. The Figures are in order of increasing d-index, with the first being Ni an alloy with a d-index of 8.0 and ending with Cu90Ni10, which has a d-index of 10.526. The right side of each figure is the RMS of the machined surface versus the cutting distance results, obtained by the methods detailed in Chapter 3.

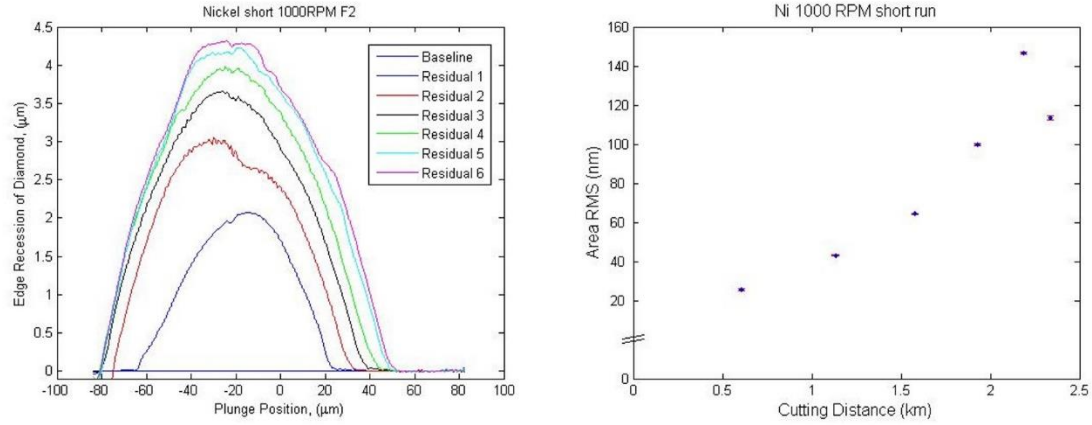


Figure 5.7: The residuals (left) of the diamond tool wear test using pure Ni, and area RMS surface finish versus Cutting Distance (right) which shows the final surface finish greater 100 nm.

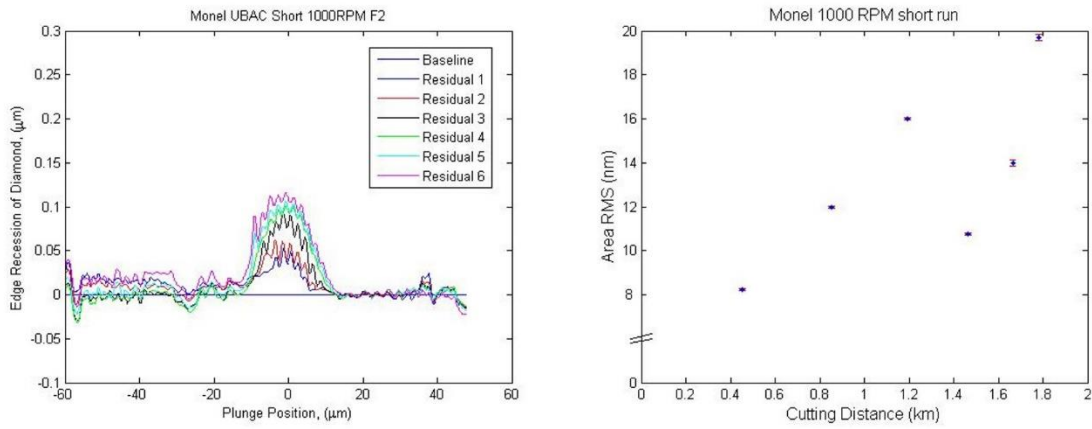


Figure 5.8: The residuals (left) of the diamond tool wear test using Monel, a Cu-Ni alloy with the second lowest d-index and second highest amount of wear tested. The RMS versus Cutting Distance (right) shows an increase of roughness as the diamond tool edge recession increases.

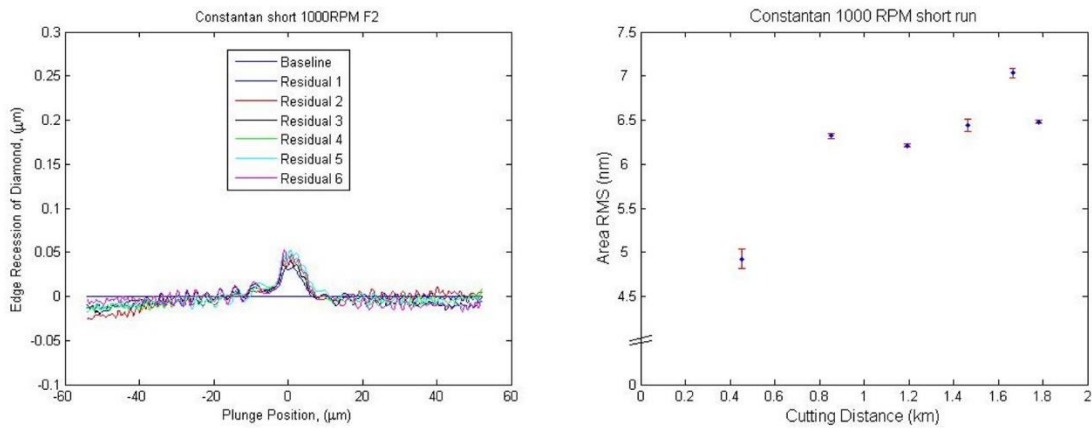


Figure 5.9: The residuals (left) of the diamond tool wear test using Constantan, a Cu-Ni alloy with the third lowest d-index. The RMS versus Cutting Distance (right) shows an increase of roughness with diamond tool edge recession.

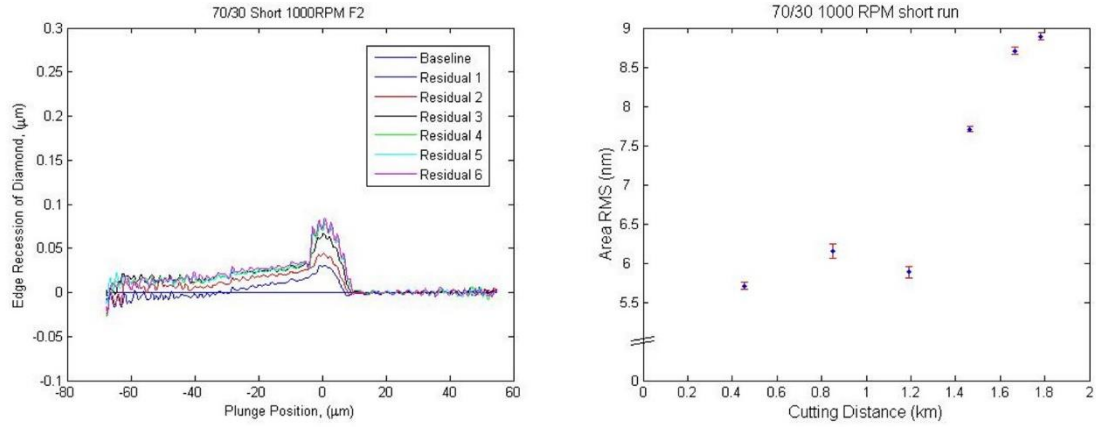


Figure 5.10: The residuals (left) of the diamond tool wear test using Cu70Ni30, a Cu-Ni alloy with the fourth lowest d-index, which has a d-index that is around the critical value dependent on the trace elements in the alloy. The RMS versus Cutting Distance (right) shows an increase of roughness as the diamond tool edge recession increases.

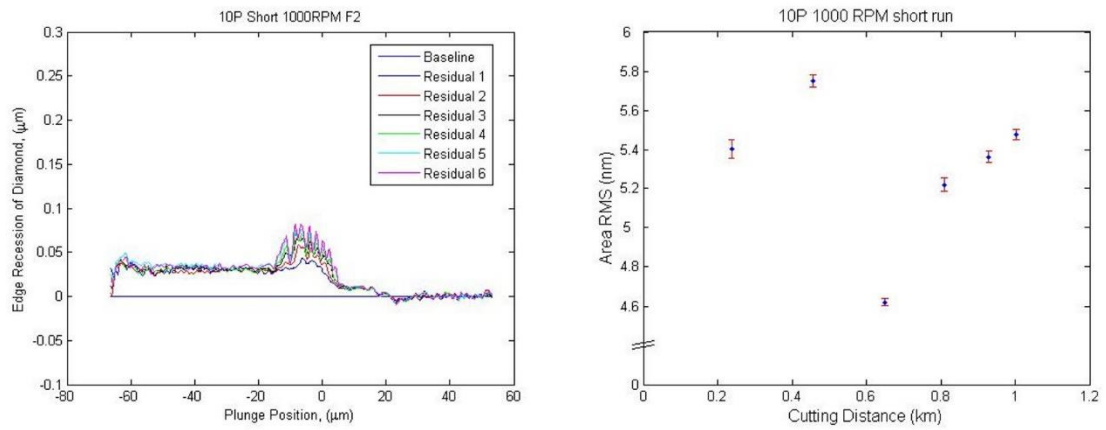


Figure 5.11: The residuals of the 10 pence coin (left) and the RMS versus Cutting distance of the workpiece (right).

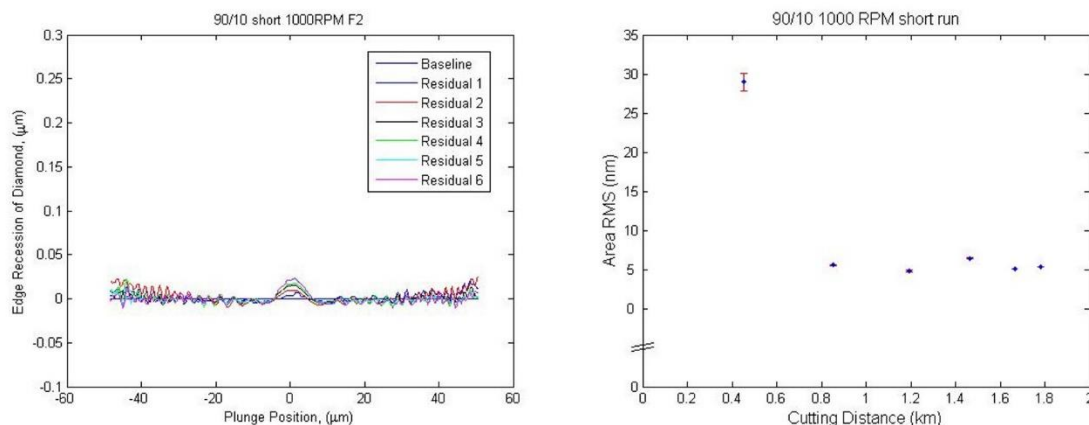


Figure 5.12: Shows the residuals of the highest d-indexed Cu-Ni alloy tested (left), and the RMS versus Cutting Distance (right).

The testing for each alloy (Figures 5.7 to 5.12) was conducted with the “short” run parameters described in chapter three; surface areas of samples were held nominally constant, except the 10p coin. In general, the expected decrease in wear with d-index (increasing Ni and trace amounts Mn and Fe) was observed. However, there are anomalies which require further work. Constantan, which is ductile and has no Mn and Fe, but had a d index less than 10 shows lower wear than Cu70Ni 30. . The 10 Pence coin showed higher levels of chemical tool wear than predicted since it has only 25 wt% Ni and a d-index above 10.

The 10 Pence coin showed higher levels of chemical tool wear than predicted since it has only 25 wt% Ni and a d-index above 10. Energy-dispersive X-ray spectroscopy (EDS) was conducted on the 10 Pence coin and the Ni content was reported to be higher (around 35 wt%) which might explain the increased leading edge recession. It was brought to attention via private communication with Dr. Tom Childs, that a nickel-oxide layer can be formed²⁸ and thus increase the amount of Ni present within EDS

reading In the presence of high nickel, copper-nickel alloys with a thickness of several microns deep. With a higher acceleration voltage, the excited nickel oxide layer will report a higher than expected percentage of nickel. EDS measurements were also made on Monel, Cu70Ni30, and Cu90Ni10, all of which show a nickel rich surface (Table 5.1). Shimada²⁵ showed increasing diamond erosion rates at elevated temperature from vacuum to modest oxygen pressures. He also showed that OFHC copper gave higher diamond tool wear than commercially pure copper, an observation he attributed to oxygen catalysis. Further analyses are required.

Table 5.1: The Percent weight composition of Cu-Ni alloys, as measured by Energy-dispersive X-ray Spectroscopy (EDS)

	Cu (wt%)	Ni (wt%)	Mn (wt%)	Fe (wt%)
90/10	83	16	0	0
10P	65	35	0	0
70/30	54	45	1	< 1
Monel	24	73	1.4	< 1

Figure 5.13 combines the final residual for each alloy tested under these conditions.

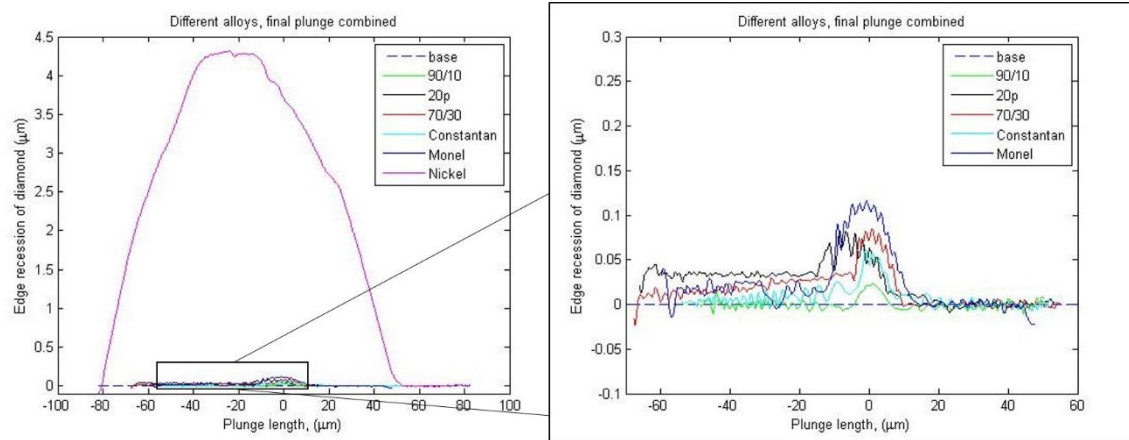


Figure 5.13: The combined final residual of each alloy, with an emphasis on the less aggressive diamond tool wearing alloys highlighted on the right.

5.4 Feedrate Testing

Tool temperature and hence chemical wear rates will be influenced by surface speed and feed rate. 2 micrometers a revolution, or 2 mm/min at 1000 rpm was selected as a baseline for this work. Tool edge recession is shown in (Figure 5.8) and at 5 μm/rev (Figure 5.14), 10 μm/rev (Figure 5.15), and 15 μm/rev (Figure 5.16). The surface velocity remained the same for different feed rates, but the cutting time decreased and distance cut decreased. (Table 3.5).

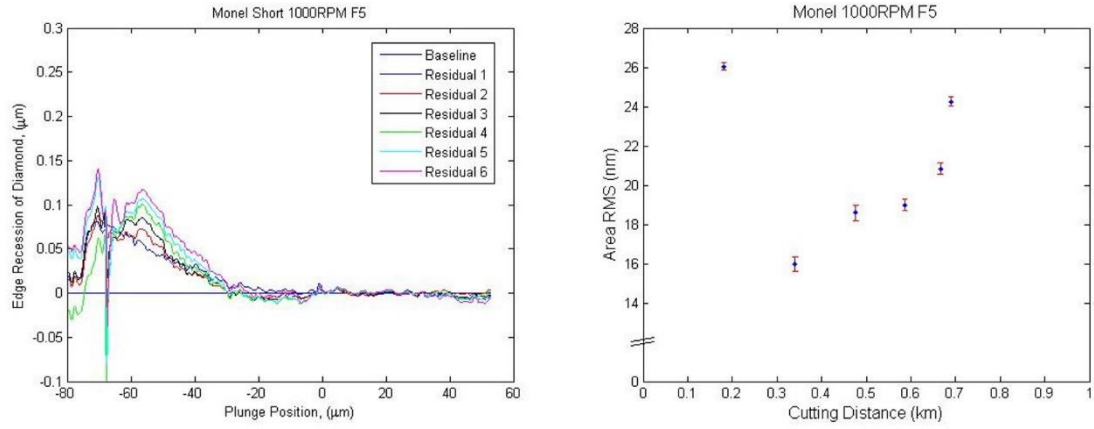


Figure 5.14: The residuals and surface finish vs. cutting distance of diamond turned Monel with a spindle speed of 1000 RPM and a Feedrate of 5 micrometers a revolution.

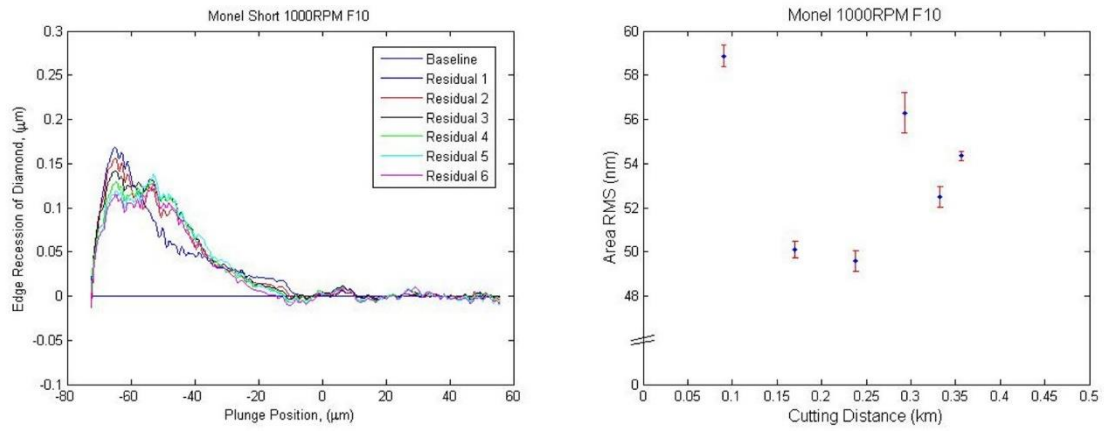


Figure 5.15: The residuals and surface finish vs. cutting distance of diamond turned Monel with a spindle speed of 1000 RPM and a Feedrate of 10 micrometers a revolution.

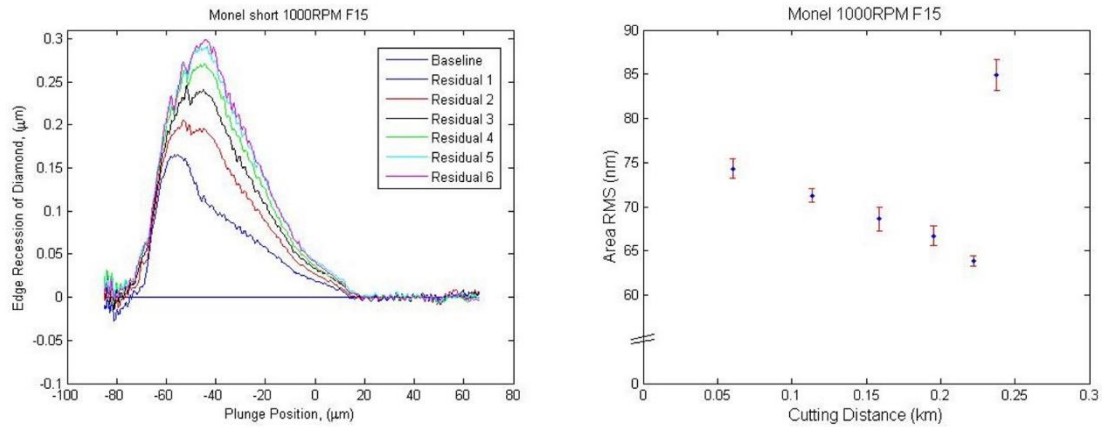


Figure 5.16: The residuals and surface finish vs. cutting distance of diamond turned Monel with a spindle speed of 1000 RPM and a Feedrate of 15 micrometers a revolution.

The final tool replications or total edge-recession per test is shown in Figure 5.17. The increase of the feedrate contributes to an increase in leading edge-recession. The 2 micrometer per revolution test shows nose-flattening is the dominant wear mechanism in these conditions, but not significant at higher feed rates. This reinforces the earlier suggestion that nose flattening is associated with very small uncut chip thicknesses.

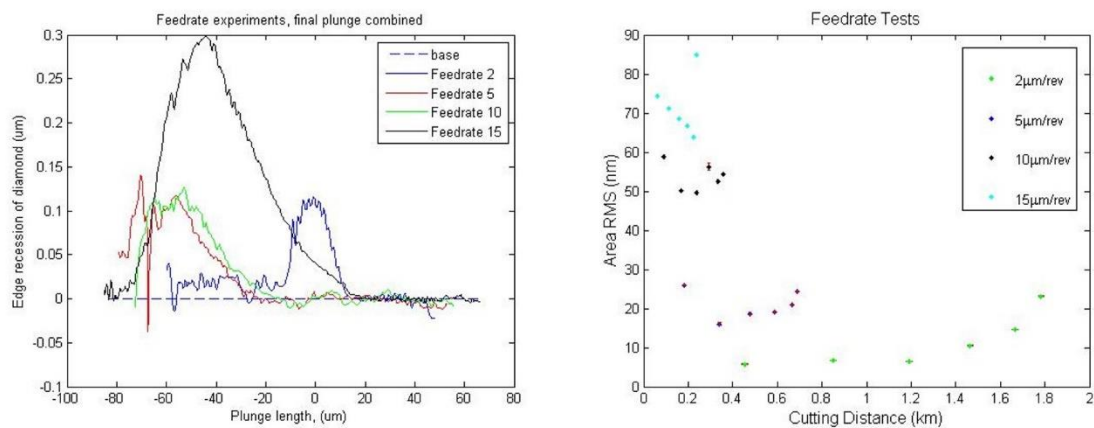


Figure 5.17: The combined Final Plunges of the diamond tool wear residuals and combined RMS vs. Cutting Distance.

Shimada et al.²⁵ showed an image of crater wear on a diamond tool when machining OFHC copper. Crater wear in conventional tool materials is normally

attributed to erosion by the chip resulting from reduced hot hardness. The rake faces of diamond tools used to machine Monel, under the conditions discussed above, were measured with the ZeGage™ (SWLI) with the 20x objective, Figure 5.18 shows the crater from the test at a feed rate of 5 $\mu\text{m}/\text{rev}$.

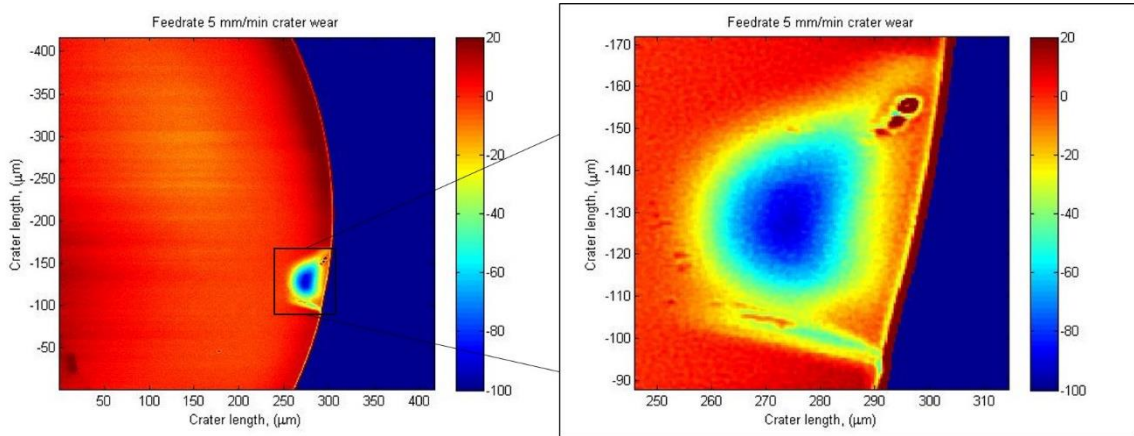


Figure 5.18: The Crater wear of the diamond tool while conducting the 5 micrometer per revolution test on Monel, height in nm.

As the feedrate increases the depth of the crater decreases but the area increases (Figure 5.19). This suggests that as time in contact with the workpiece increases (i.e. decreased feed rate) so does the catalytic diamond tool wear, which seems reasonable for a surface reaction.

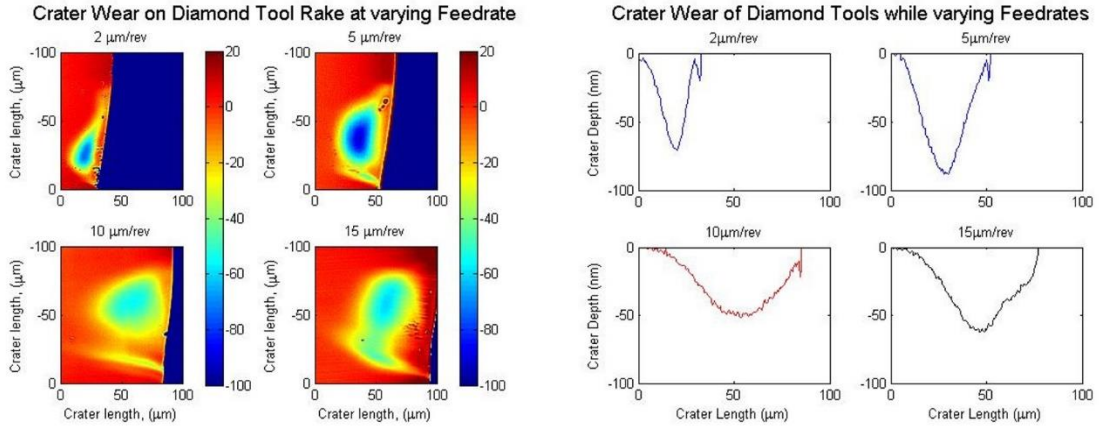


Figure 5.19: The rake face of the four diamond tools used for each feedrate variation (left) with the height in nanometers, and a profile taken across the deepest point of the crater in each tool normal to the cutting edge.

The crater on the rake face of the diamond tool changes shape as the feed rate changes. This may be attributed to increasing temperature with increasing feed per revolution as well as changes in the chip shape and perhaps morphology (powdery segmented chips vs continuous chips). With increasing feed rate, the depth of the crater decreases and the crater elongates. A leading edge notch become more apparent and deeper as feed rate increases.

5.5 Variation of Surface Velocity

In the current experimental configuration separation of effects of feedrate, surface speed and time is difficult. A series of tests were performed in which the average surface velocity of the workpiece (i.e. the spindle speed) was varied while the feedrate per revolution was held constant at 2 $\mu\text{m}/\text{rev}$. The time to turn each band also varied as the spindle speed was changed. The crater wear on the diamond tool for this set of tests showed that as the average velocity of the band increased so did the depth of the crater, as seen in Figure 5.20. Figure 5.21 shows the halved velocity and cutting time residuals and

RMS versus cutting distance. Figure 5.8 is the baseline experiment, while Figure 5.22 average velocity was doubled all other things held constant.

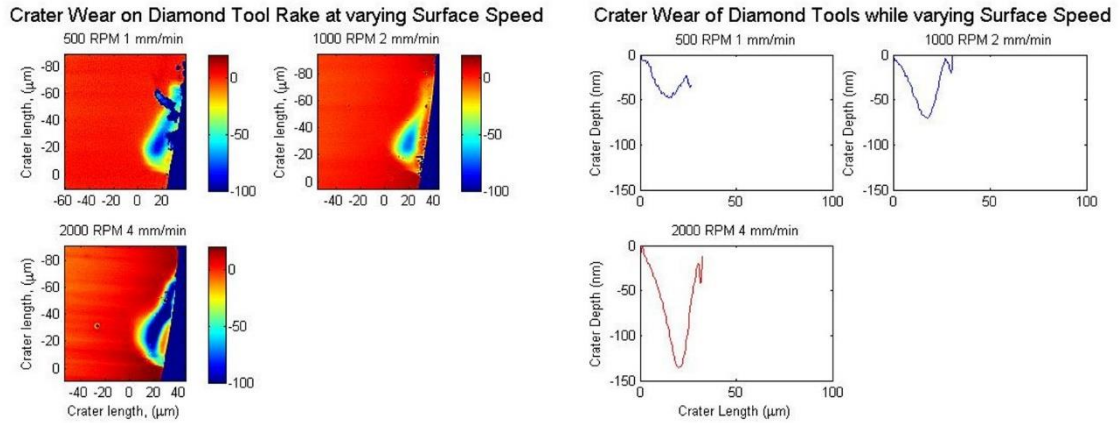


Figure 5.20: The crater wear on the rake face of the diamond tool with height in nanometers (left), and a profile across the most deep section of the crater (right).

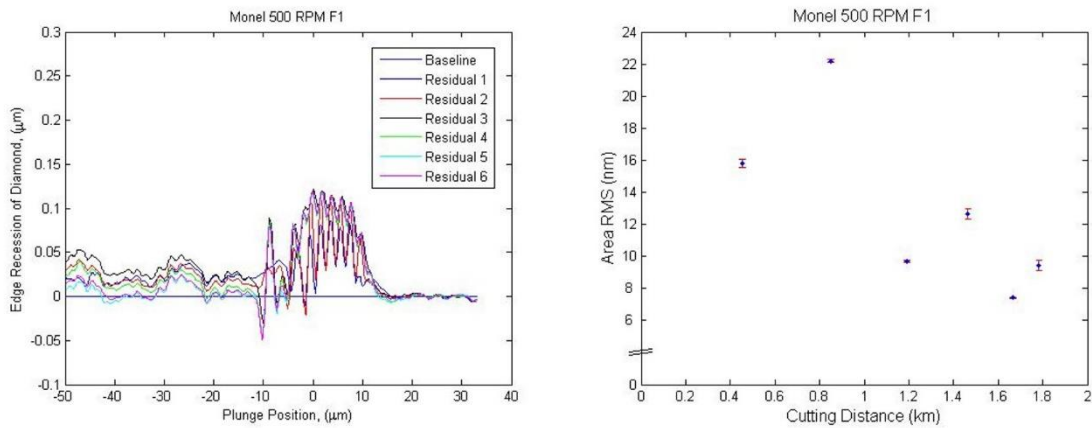


Figure 5.21: Residuals and RMS of Monel turned with 500 RPM Spindle speed and a feedrate of $2\mu\text{m/rev}$

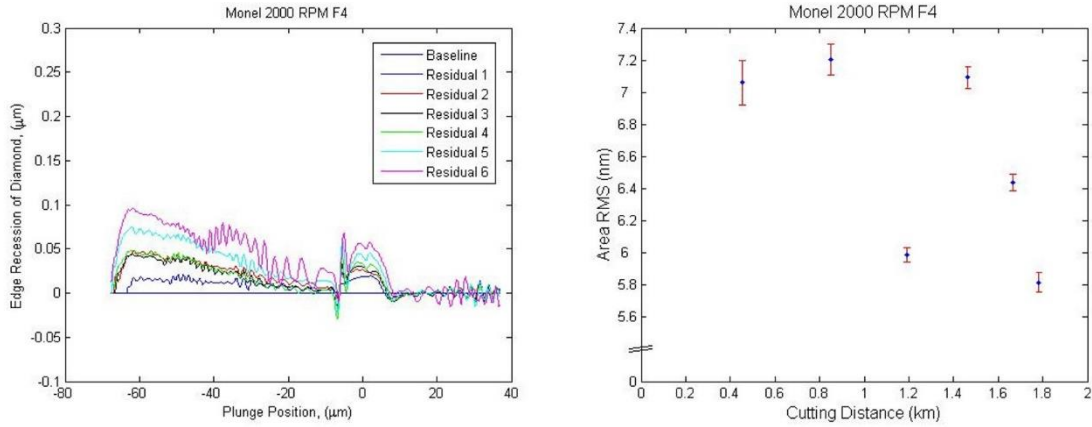


Figure 5.22: Residuals and RMS of Monel turned with 2000 RPM Spindle speed and a feedrate of $2\mu\text{m/rev}$

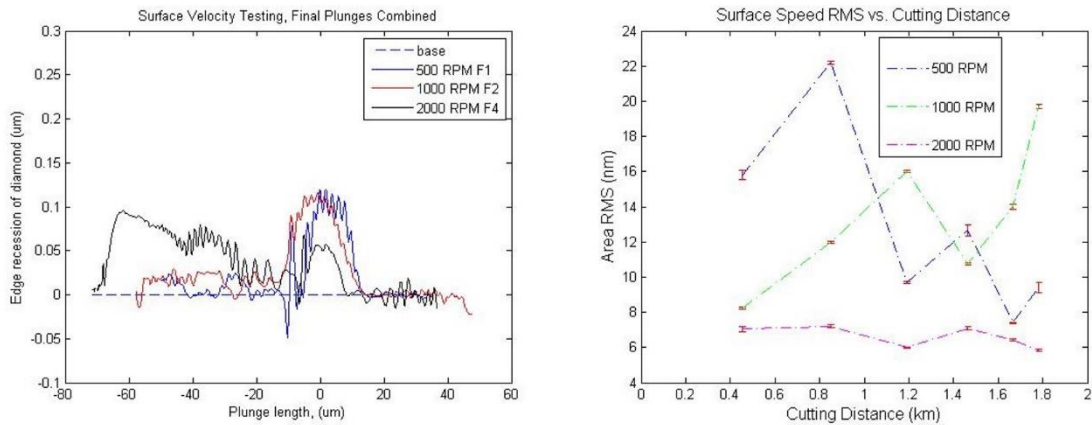


Figure 5.23: Residuals and RMS of Monel turned with varying surface speeds at a feed rate of $2\mu\text{m/rev}$.

Figure 5.23 combines the final replication of the diamond tool edge for all three tests varying the average velocity per band. As the average velocity increases the leading edge-recession also increases. The time that the diamond tool is in contact with the workpiece decreases as the average velocity increases in these tests, but the chemical wear is increased. The nose rubbing of the 500 RPM test shows a deeper set of grooves than the tests with higher surface speed.

5.6 Constant Time Tests

The following set of tests were taken in order to determine what would occur if the time per test was held constant as the average velocity changed per band. This caused a change in cutting distance. The baseline test results shown in Figure 5.8, Monel diamond turned with a spindle speed of 1000 RPM and a feedrate of $2\mu\text{m}/\text{rev}$. The Feedrate in millimeters per minute was held constant, changing the spindle speed to 500 RPM and the feedrate to $4\mu\text{m}/\text{rev}$ (Figure 5.24). The other end was to increase the spindle speed to 2000 RPM and decreasing the feedrate to $1\mu\text{m}/\text{rev}$ (Figure 5.25). Figure 5.26 is the combination of the last plunges with of each test, and the RMS versus cutting distance of all of the tests. The most noticeable trend is that as the cutting velocity and distance are increased the amount of nose rubbing increases, and the groove formation also becomes more drastic with the higher cutting distance.

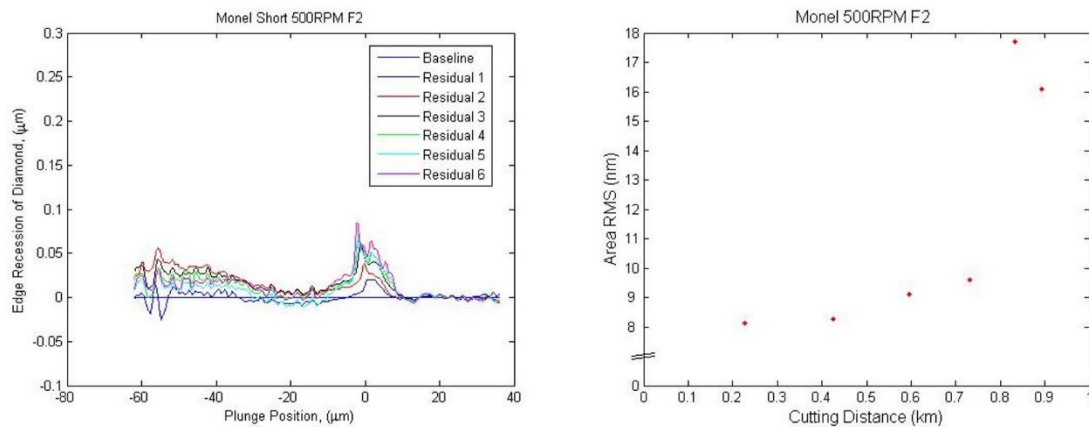


Figure 5.24: Residuals and RMS of Monel turned with 500 RPM Spindle speed and a feedrate of $4\mu\text{m}/\text{rev}$.

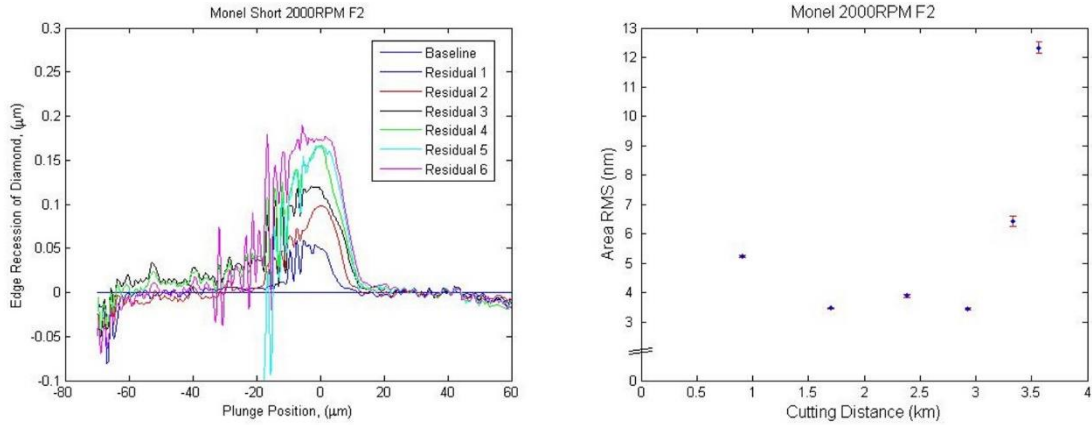


Figure 5.25: Residuals and RMS of Monel turned with 2000 RPM Spindle speed and a feedrate of $1 \mu\text{m}/\text{rev}$.

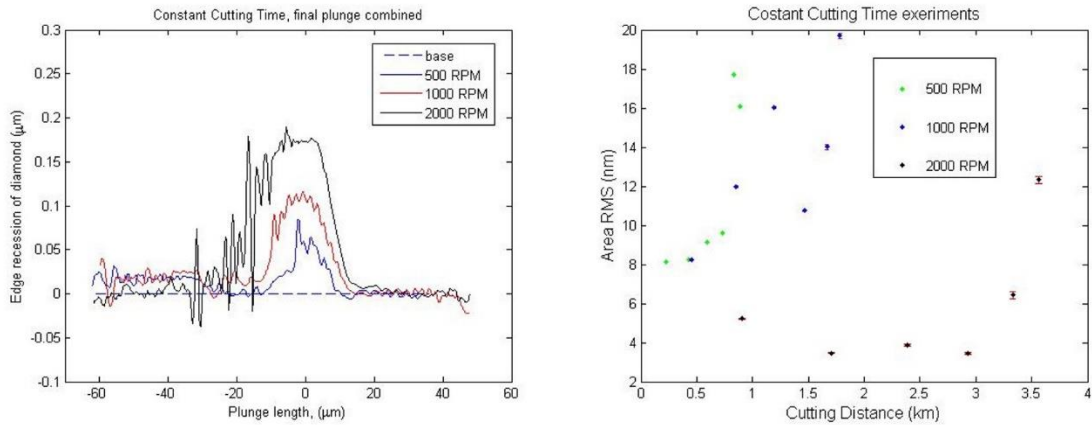


Figure 5.26: Combined Residuals and RMS vs. Cutting Distance of constant time tests in Monel.

5.7 Uncertainty

A detailed uncertainty analysis has not been performed. Contributions from the SWLI measurements were discussed in Chapter 3. An indication of the reproducibility of the measurements of the wear is obtained from the processing of data acquired at 4 different locations on the UBAC witness sample. Figure 5.27 shows a plot of the maximum, minimum, average, and the standard deviation by location of the four measurements. Taking the standard deviation of the standard deviation vector giving a

total sigma of 1.9 nanometer for the difference of location on the witness sample, with a maximum standard deviation of 10 nm and an average standard deviation of 2.9 nm.

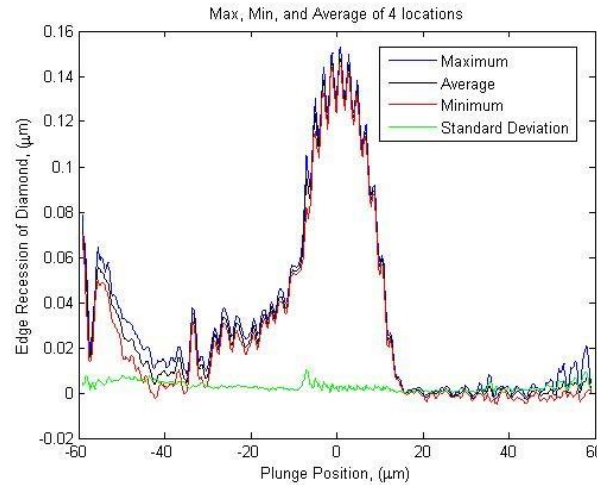


Figure 5.27: The minimum, maximum, and average difference of measurements at different locations on the witness sample giving a total standard deviation of the location on the witness sample of 1.9 nanometers

Since fine alignment is performed using the nominally unworn portion of the tool in MatLab, the extrapolation will cause increasing uncertainty. Uncertainty also increases for the highly worn tools, where there may be a bias arising from increased deformation and/or elastic spring back in the witness sample. This is noticeable in cases where diamond appears to be added (e.g. Figure 5.24).

For mild wear, it is difficult to locate the wear scar in a Scanning Electron Microscope (SEM). The wear scar was found for the test on Monel at 1000 rpm and a feed of 15 $\mu\text{m}/\text{rev}$ and then compared to the residual of the final plunge (Figure 5.28). A qualitative observation can be made showing the direct correlation of the physical wear scar on the diamond tool and the calculated residual replicated into the UBAC witness sample.

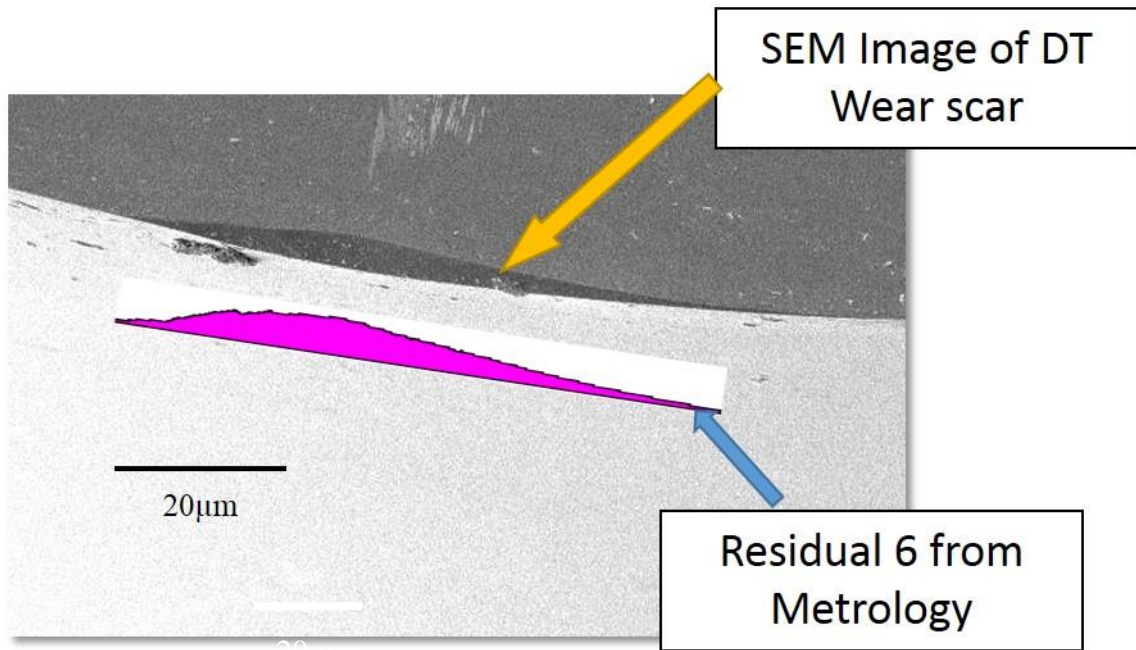


Figure 5.28: A qualitative correlation of the wear scar seen in an SEM next to residual of the same test.

CHAPTER 6: CONCLUSIONS AND FUTURE WORK

A high resolution method has been described for measuring diamond tool edge recession intermittently during a tool wear experiment without removing the tool from the machine. This enables high time (or cutting distance) resolution with no concern for tool relocation in the machine.

The SWLI based metrology technique has been applied to an experimentally convenient configuration, face turning. Following previous work, a stepped sample has been machined, allowing both tool wear and surface finish to be measured as a function of cutting distance.

The experimental technique has been applied to the binary copper-nickel alloy system, which at equilibrium, is single phased for all compositions. Wear rates have been measured as a function of composition, feed rate, surface speed, and contact time. The d-index approach suggests a monotonic increase in chemical wear rates with decreasing d-index. The experimental results support that general trend, with some anomalies. Modeling of cutting temperatures²⁹ may provide some insights based on material properties. The data developed will allow calculation of activation energies for chemical reactions between Cu-Ni alloys and diamond³⁰.

The metrology method provides nm level resolution (with uncertainties likely in the 10-20 nm range except at very high wear) of edge recession. This has allowed identification of Pecalharing grooves with periods of 2 micrometers and amplitudes of

20-50 nm, crater wear, and diamond wear propagation along defect planes in the diamond. Future work includes changing from facing to turning. This will require minor adaptation of the analysis (Appendix 1), but will provide constant surface speed throughout an experimental run. Chapter 5 shows a plausible correlation between the measured edge recession and an SEM image of tool wear at the end of a test.

Development of an independent procedure for capturing the tool shape change during an experimental run is recommended possibly through static replication techniques.

The theory of a sharp increase of chemical diamond wear when the d-index is 10 is not as definitive as originally expected, however the trend of chemical wear increases as expected. Further investigation is required to determine the source of the anomalies.

REFERENCES

1. Rhorer, R. and Evans, C. "Fabrication of optics by diamond turning," in OSA Handbook of Optics, 2nd Ed., Vol. 1, Washington, DC: McGraw-Hill, 1995
2. Evans, C. J. Precision Engineering: An Evolutionary View. Cranfield, UK: Cranfield Press, 1989
3. Evans, C. J. "Cryogenic diamond turning of stainless steel," Annals CIRP, 1991 40, 571-5
4. Hurt, H.H and Decker, D.L. "Tribological Considerations of the Diamond Single-Point Tool," SPIE, Vol. 508, pgs. 136-131, 1984
5. Syn, C. K., Taylor, J. S. and Donaldson, R. R. "Diamond tool wear vs. cutting distance on electroless nickel mirrors," Proc SPIE, 1986, 676, 128-140
6. Paul E, Evans CJ, Mangamelli A, McGlauffin ML, Polvani RS. "Chemical aspects of tool wear in single point turning," Precision Engineering 1996; 18:4-19
7. Okamoto, H. "Desk Handbook: Phase Diagrams for Binary Alloys," ASM International, 2000
8. Brookes, C. and Zhang, L., "Cumulative deformation and fatigue of diamond – new development," Diamond and Related Materials, v 8, n 8-9, p 1515-21, Aug. 1999
9. Ueda, T. Sato, M. Nakayama, K. "The temperature of a single crystal diamond tools in turning," CIRP Annals Manufacturing Technology 47 (1998) 41–44.
10. Shimada, S., Inamura, M., Tanaka, H., "Suppression of Tool Wear in Diamond Turning of Copper under Reduced Oxygen Atmosphere," Annals CIRP, 2000, Vol 49, pgs. 21-24
11. Taylor, J. S., Syn, C. K., Saito, T. T. and Donaldson, R. R., "Surface finish measurements of diamond-turned electroless-nickel-plated mirrors," Opt Eng, 1986, 25, 1013-1020
12. Dini, J. W., Donaldson, R. R., Syn, C. K. and Sugg, D. J. "Diamond tool wear of electrodeposited nickel phosphorus alloy," Proc SUR/FIN '90 (American Electroplaters and Surface Finishers Society, 1990)
13. Evans, C. J., Polvani, R. S. and Mayer, A. Diamond Turned Electro-Deposited Nickel. Monterey, CA: OF&T, 1989

14. Evans, C., Paul, E., "Catalytic Chemical Wear of Diamond Tools while Cutting Alloys," National Science Foundation Proposal
15. M.Shi, B.Lane, C.B.Mooney, T.A.Dow, R.O.Scattergood, "Diamond tool wear measurement by electron-beam-induced deposition," *Precision Engineering* 34 (2010)718–721
16. GRIFFIN, A. Senior Design project, UNC Charlotte 2011
17. E. Brinksmeier, R. Gläbe, "Advances in Precision Machining of Steel," *Annals of the CIRP*, 50/1 (2001), pp. 385–388
18. Decker, D. L. , Hurt, H. H. , Dancy, J. H. , and Fountain, C. W. , "Preselection of Diamond Single-Point Tools," *Proc. of the SPIE*, 1984
19. L. Deck and P. de Groot, "A new high-speed non-contact profiler based on scanning white light interferometry," *Proc. ASPE* 424-426 (1993)
20. J. Troutman, C. Evans, and T. Schmitz, "Vibration Effects on an Environmentally Tolerant Scanning White Light Interferometer," *ASPE* 2013
21. Liesener, J., Evans, C., De Groot, P., *Proceedings - ASPE 2011 Annual Meeting*, v 52, p 23-26, 2011
22. Bernasconi, K., Summer research project, 2013, testing on Rupert standards
23. Measurements Taken by M. Farsad 2014
24. Brinksmeier, E., Gläbe, R., Lünemann, B., "Manufacturing of diffractive microstructures using an open loop nanometer-stroke Fast Tool Servo system." *Proc. of the 10th EUSPEN Conference*, Zurich, May 2008, pp. 125 – 128
25. S.Shimada, H.Tanaka, M.Higuchi, T.Yamaguchi, S.Honda, K.Obata, "Thermo-chemical wear mechanism of diamond tool In machining of ferrous metals," *CIRP Annals Manufacturing Technology*, 53 (2004), 57–60
26. Evans, C. and Bryan, J., "Structured', 'textured' or 'engineered' surfaces," *CIRP Annals - Manufacturing Technology*, v 48, n 2, p 541-556, 1999
27. Pekelharing, A., "Material Side Flow in Finish Turning," *CIRP Annals*, Vol. 20, 1972, 21-22
28. Castle, J. and M. Nasserian-Riab, "The Oxidation of Cupronickel alloys-I. XPS Study of Inter-Diffusion," *Corrosion Science*, 1975, Vol. 15, pp. 537 to 543
29. Personal communication with Dr. Tom Childs, 2014

30. Personal communication with Dr. Ed Paul, 2014

APPENDIX: MATLAB CODE

RMS versus Cutting Distance

```

% RMS v CD with error bars
clc
clear all
close all
%% CD Short
r=19.9;
fr=.002;
rpm=1000;
cd1=((19.9^2)-(10.4^2))*pi/((.002*1000);
cd2=cd1+((19.9^2)-(11.9^2))*pi/((.002*1000);
cd3=cd2+((19.9^2)-(13.4^2))*pi/((.002*1000);
cd4=cd3+((19.9^2)-(14.9^2))*pi/((.002*1000);
cd5=cd4+((19.9^2)-(16.4^2))*pi/((.002*1000);
cd6=cd5+((19.9^2)-(17.9^2))*pi/((.002*1000);
cd=[cd1 cd2 cd3 cd4 cd5 cd6]*10^-3;
%% This is to make a graph with error bars
%band 1
band1a=5.93;
band1b=5.35;
band1c=6.66;
band1d=5.06;
all_1=[band1a band1b band1c band1d];
x1=nanmean(all_1);
e1=std(all_1);
%band 2
band2a=7.23;
band2b=6.14;
band2c=7.28;
band2d=6.44;
all_2=[band2a band2b band2c band2d];
x2=nanmean(all_2);
e2=std(all_2);
%band 3
band3a=6.99;
band3b=5.05;
band3c=7.31;
band3d=6.39;
all_3=[band3a band3b band3c band3d];
x3=nanmean(all_3);
e3=std(all_3);
%band 4
band4a=10.89;
band4b=10.15;
band4c=11.29;
band4d=9.67;
all_4=[band4a band4b band4c band4d];
x4=nanmean(all_4);
e4=std(all_4);
%band 5
band5a=14.93;
band5b=14.52;
band5c=15.24;
band5d=13.55;

```

```

all_5=[band5a band5b band5c band5d];
x5=nanmean(all_5);
e5=std(all_5);
%band 6
band6a=22.42;
band6b=22.01;
band6c=24.06;
band6d=23.98;
all_6=[band6a band6b band6c band6d];
x6=nanmean(all_6);
e6=std(all_6);
x=[x1 x2 x3 x4 x5 x6];
e=[e1 e2 e3 e4 e5 e6]*10^-1;
figure
h=errorbar(cd,x,e,'Color','r');
xlabel('Cutting Distance (km)','fontsize',12);
ylabel('Area RMS (nm)','fontsize',12);
xlim([0 2.0])
% Enter the title below
title('Monel 1000 RPM short run','fontsize',12);
set(h,'linestyle','none')
yTickOld = get(gca,'Ytick');
dYtick = abs(diff(yTickOld));
yTickNew = [yTickOld(1)-2*dYtick(1) yTickOld];
set(gca,'Ytick',yTickNew)
yTickLabelOld = get(gca,'Yticklabel');
yTickLabelNew = {'0';''};
for i = 1:length(yTickLabelOld)
    yTickLabelNew(i+1) = {yTickLabelOld(i,:)};
end
set(gca,'yLim', [yTickNew(1) yTickNew(end)])
set(gca,'Yticklabel',yTickLabelNew)
xLimits = get(gca,'xlim');
posGCA = get(gca,'Position');
yHeight = 1/length(yTickNew)*posGCA(4);
annotation(gcf,'line',[posGCA(1) posGCA(1)],...
    [posGCA(2)+yHeight*.95 posGCA(2)+yHeight*1.05],...
    'LineWidth',1,'Color',[.999 .999 .999]);
annotation(gcf,'line',[posGCA(1)-posGCA(3)/40
    posGCA(1)+posGCA(3)/40],...
    [posGCA(2)+yHeight posGCA(2)+yHeight*1.1], 'LineWidth',1);
annotation(gcf,'line',[posGCA(1)-posGCA(3)/40
    posGCA(1)+posGCA(3)/40],...
    [posGCA(2)+yHeight*.9 posGCA(2)+yHeight], 'LineWidth',1);
set(gca,'yLim', [yTickNew(1) yTickNew(end)])
set(gca,'xLim', xLimits)
set(gca,'Yticklabel',yTickLabelNew)
hold on
plot(cd,x,'.b')

```

Dat 2 Mat

```

function [PhaseMap]=Dat2Mat(filename)
lError=0;
DatInFileName1=strcat(filename);
[lError1,
InfoHeader1,IntensityMap1,PhaseMap1]=ReadMetroProFile(DatInFileName1);

```

```
PhaseMap=PhaseMap1.*1e9;% nm
```

Rotate Data

This is to rotate images

```
function [PhaseMap]=rotatedata(PhaseMap,smaller,larger)
%PhaseMap is the data to be rotated
%first select a point on the top and the bottom that should linear and
%vertical but is rotated, the smaller value is the input: smaller, the
%larger value is the input: larger
ypixelcount=1024;%the number of pixels in the detector in the y
direction
rotAngle= atand((smaller-larger)/ypixelcount); %<-----need to go to
previous figure and find two points
PhaseMap=imrotate(PhaseMap,rotAngle,'bilinear','crop'); %rotates the
phase %map so that the "edge" is vertical( this is a function in the
image %processing toolbox
```

Tilt Removal

```
%% removing plane
function [PhaseMap]=removetilt(PhaseMap,levelingright,levelingleft)
%PhaseMap is from reading raw data into Matlab
% levelingright is selected left limit to remove tilt
% levelingleft is selected right limit to remove tilt
refPlane=PhaseMap(:,levelingright:levelingleft);
gridSize=size(refPlane);
[x,y] = meshgrid(1:1:gridSize(2),1:1:gridSize(1));
i = find(~isnan(refPlane));%find good data
X=x(i); %vectors of locations of good data
Y=y(i);
Z=refPlane(i);
fit=[ones(size(X)) X Y];% model
A=fit\Z;%coefficients of the best fit plane
bestfit=ones(size(x));%array of ones
bestfit=bestfit.*A(1)+x.*A(2)+y.*A(3);
gridSize=size(PhaseMap); %size of reference plane
[x,y] = meshgrid(1:1:gridSize(2),1:1:gridSize(1));%generate x- and y-
matrices for fitting
bestfit7=ones(size(PhaseMap));%array of ones
bestfit7=bestfit7.*A(1)+x.*A(2)+y.*A(3); % generate best fit plane for
the tilted reference
PhaseMap=PhaseMap-bestfit7;
```

Rough Centering and Data Truncation

```
function [ x,p,plunge ] = datachop( filename)
%THIS function chops the data from each plunge and sets it up to be
%processed and plotted via a waterfall plot.
PhaseMap=Dat2Mat(filename);
%PhaseMap Figure of Raw data
B=PhaseMap; % THIS is the Phasemap in nm from the dat2mat
%plot profiles to get cropping
h=figure; %**Figure of array across the top of
%plunge
plot (PhaseMap(20,:))
title('top row for rotational alignment, select top left edge of
plunge')
```

```

ylabel('depth of plunge (nm)')
xlabel('pixels')
pause(0.001) %<== Adding this line made it all work...
jf=get(h, 'JavaFrame');
set(jf, 'Maximized',1);
[x,y]=ginput(1); %this is the code that selects the top place on the
plunge
j=figure;
plot (PhaseMap(1010,:) ) %bottom row alignment
title('bottom row for rotational alignment, select top left edge of
plunge')
ylabel('depth of plunge (nm)')
xlabel('pixels')
pause(0.001) %<== Adding this line made it all work...
jf=get(j, 'JavaFrame');
set(jf, 'Maximized',1);
[r,f]=ginput(1);
% for g input select the top left of each plunge on the 2 plot image
%this does the imrotate of the phasemap
% rotate raw data, angle obtained manually
smaller=x(1); %on left side of top and bottom select point for
rotation
larger=r(1); %on left side of top and bottom select point for rotation
PhaseMap=rotatedata(PhaseMap,smaller,larger);
%Plot of rotated PhaseMap
n=nanmean(PhaseMap); % column average of the phasemap
p=figure;
plot(n);
title('cropping plot, select the left limit and right limit of the
flats')
ylabel('depth of plunge (nm)')
xlabel('pixels')
pause(0.001) %<== Adding this line made it all work...
jf=get(p, 'JavaFrame');
set(jf, 'Maximized',1);
[s,v]=ginput(2); % the section where you select the data left and right
rlim=s(1);
llim=s(2);
%% remove tilt
ref=ones(size(PhaseMap)); %A matrix of 1's the size of the PhaseMap
ref(:,rlim:llim)=nan; %setting the internal points of the selection
to Nan
fitplane=ref.*PhaseMap; %Multiplying ones by phasemap
refPlane=fitplane;
gridSize=size(refPlane);
[x,y] = meshgrid(1:1:gridSize(2),1:1:gridSize(1));%mesh the size of
phasemap
i = find(~isnan(refPlane));%find good data
X=x(i); %vectors of locations of good data
Y=y(i);
Z=refPlane(i); %only good data
fit=[ones(size(X)) X Y];% model
A=fit\Z;%coefficients of the best fit plane
bestfit=ones(size(x));%array of ones
bestfit=bestfit.*A(1)+x.*A(2)+y.*A(3);%multiplying by the fit
coefficients
gridSize=size(PhaseMap); %size of reference plane

```



```

[x,y] = meshgrid(1:1:gridSize(2),1:1:gridSize(1));%generate x- and y-
matrices for fitting
bestfit7=ones(size(PhaseMap));%array of ones
bestfit7=bestfit7.*A(1)+x.*A(2)+y.*A(3); % generate best fit plane for
the tilted reference
PhaseMap=PhaseMap-bestfit7; %removing the tilt from the data
%% Section to remove the flats
%THis chops the excess data off
g=nanmean(PhaseMap); %column average of phasemap
m=figure;
plot(g)
title('remove flats, select the left limit then right limit of the
plunges')
ylabel('depth of plunge (nm)')
xlabel('pixels')
pause(0.001) %<== Adding this line made it all work...
jtf=get(m, 'JavaFrame');
set(jtf, 'Maximized',1);
[x,y]=ginput(2);
rlim=x(1);
llim=x(2);
plunge=(PhaseMap(11:1014,rlim:llim)); %trim Trimming the phsemap
close all % closes all screens
%% Center in X on unworn section of plunge
p0=nanmean(plunge); %Column Average of the Plunge (1024)
spacing=0.1; %The amount to interpolate between data points
dx=417/1024; %417 um field of view divided by the amount of pixels
p0i=p0*10^-5;%puts data in um *****possible issue
x00=dx*(1:1:length(p0));% x vector to go with plunge
% p0i=interp(p0,10); %interpolates data with 10 points between
size(p0); %tells the size of the data
figure %figure plotted to select data
p01=p0i*10^2
plot(p01')
title('plunge , select worn data to remove')
ylabel('depth of plunge (\mum)')
xlabel('pixels')
[m,n]=ginput(2);
drop=m(2)-m(1);%data selected to skip when averaging
p=p0i;
p(m(1):m(2))=nan; % makes the values between the plots = to NaN
dxx=(417/1024); %the spacing of tenth pixels
x=dxx*(1:1:length(p));% x vector to go with plunge
k=nanmean(x); %mean of data not removed
x0=x-k; %subtracting the mean from the x vector in the data
x=x0;
p=p0i;
close all
end

```

Final Data Analyses

```

%clear all
close all
clc
filename='Monel_20x_1000_short_a_plunge1.dat';

```

```

[x,p,plunge]=datachop_function_v3(filename);
x0=x;
p0=p;
plunge0=plunge;
%%
filename='Monel_20x_1000_short_a_plunge2.dat';
[x,p,plunge]=datachop_function_v3(filename);
x1=x;
p1=p;
plunge1=plunge;
%%
filename='Monel_20x_1000_short_a_plunge3.dat';
[x,p,plunge]=datachop_function_v3(filename);
x2=x;
p2=p;
plunge2=plunge;
%%
filename='Monel_20x_1000_short_a_plunge4.dat';
[x,p,plunge]=datachop_function_v3(filename);
x3=x;
p3=p;
plunge3=plunge;
%%
filename='Monel_20x_1000_short_a_plunge5.dat';
[x,p,plunge]=datachop_function_v3(filename);
x4=x;
p4=p;
plunge4=plunge;
%%
filename='Monel_20x_1000_short_a_plunge6.dat';
[x,p,plunge]=datachop_function_v3(filename);
x5=x;
p5=p;
plunge5=plunge;
%%
filename='Monel_20x_1000_short_a_plunge7.dat';
[x,p,plunge]=datachop_function_v3(filename);
x6=x;
p6=p;
plunge6=plunge;
%%
file='Raw_data_centered_truncated.mat';
save(file,'x0','x1','x2','x3','x4','x5','x6','p0','p1','p2','p3','p4','p5','p6');
yscale=2; %to put into the right units of microns
p0=p0*10^yscale; %plunge 0 in microns
p1=p1*10^yscale; %plunge 1 in microns
p2=p2*10^yscale; %plunge 2 in microns
p3=p3*10^yscale; %plunge 3 in microns
p4=p4*10^yscale; %plunge 4 in microns
p5=p5*10^yscale; %plunge 5 in microns
p6=p6*10^yscale; %plunge 6 in microns
figure % The figure to plot the plunges in order to select the left and
plot(x0,p0) %right limit of the plunges
hold on
plot(x1,p1)
plot(x2,p2,'r')

```

```

plot(x3,p3,'k')
plot(x4,p4,'g')
plot(x5,p5,'c')
plot(x6,p6,'m')
hold off
title('Combined Plunges')
xlabel('Plunge Position (\mum) ')
ylabel('Plunge Depth (\mum) ')
legend('plunge0','plunge1','plunge2','plunge3','plunge4','plunge5',...
       'plunge6','Location','Best')
[m,n]=ginput(2); %user selection by left clicking the left limit
lcut=round(m(1));%data to drop left limit
rcut=round(m(2));%data to drop right limit
spacing=.001; %amount to interpolate points between data points to make
the
%same length in order to find residuals
xint=lcut:spacing:rcut; %x-vector for new interpolated data with 100
points
p0i=interp1(x0,p0',xint','linear'); %linear interpolation of plunge 0
p1i=interp1(x1,p1',xint','linear'); %linear interpolation of plunge 1
p2i=interp1(x2,p2',xint','linear'); %linear interpolation of plunge 2
p3i=interp1(x3,p3',xint','linear'); %linear interpolation of plunge 3
p4i=interp1(x4,p4',xint','linear'); %linear interpolation of plunge 4
p5i=interp1(x5,p5',xint','linear'); %linear interpolation of plunge 5
p6i=interp1(x6,p6',xint','linear'); %linear interpolation of plunge 6
%% memory Management
clearvars -except xint p0i p1i p2i p3i p4i p5i p6i spacing file
%% Subtracting The intial plunge giving the residuals
p0n=p0i-p0i; %initial plunge subtracted from itself
p1n=p1i-p0i; %initial plunge subtracted from plunge 1
p2n=p2i-p0i; %initial plunge subtracted from plunge 2
p3n=p3i-p0i; %initial plunge subtracted from plunge 3
p4n=p4i-p0i; %initial plunge subtracted from plunge 4
p5n=p5i-p0i; %initial plunge subtracted from plunge 5
p6n=p6i-p0i; %initial plunge subtracted from plunge 6
%% Residuals
figure %plot of the residuals roughly aligned
plot(xint,p0n)
hold on
plot(xint,p1n)
plot(xint,p2n,'r')
plot(xint,p3n,'k')
plot(xint,p4n,'g')
plot(xint,p5n,'c')
plot(xint,p6n,'m')
title('Select the unworn section of the plunge to remove the tilt')
ylabel('Edge Recession of Diamond, (\mum)')
xlabel('Plunge Position, (\mum)')
[g,c]=ginput(2); %user selected left and right limit of unworn diamond
lfit1=round(g(1));%data to fit
rfit1=round(g(2));%data to fit
ddd=lfit1:rfit1; %in between left and right limit of unworn diamond
lfit=find(xint==lfit1); %finding index of lfit
rfit=find(xint==rfit1); %finding index of rfit
p1fit=p1n(lfit:rfit); %Plunge 1 unworn section for tilt correction
p2fit=p2n(lfit:rfit); %Plunge 2 unworn section for tilt correction
p3fit=p3n(lfit:rfit); %Plunge 3 unworn section for tilt correction

```

```

p4fit=p4n(lfit:rfit); %Plunge 4 unworn section for tilt correction
p5fit=p5n(lfit:rfit); %Plunge 5 unworn section for tilt correction
p6fit=p6n(lfit:rfit); %Plunge 6 unworn section for tilt correction
dx=417/1024; %spacing of raw data from interferometer per pixel
%% Memory Management
clear p1n p2n p3n p4n p5n p6n
%% the fitting of the selected data to determine the slope
xint2=lfit:rfit;
D=polyfit(xint2,p1fit,1); %slope of plunge 1 unworn data
E=polyfit(xint2,p2fit,1); %slope of plunge 2 unworn data
F=polyfit(xint2,p3fit,1); %slope of plunge 3 unworn data
G=polyfit(xint2,p4fit,1); %slope of plunge 4 unworn data
H=polyfit(xint2,p5fit,1); %slope of plunge 5 unworn data
I=polyfit(xint2,p6fit,1); %slope of plunge 6 unworn data
%% Slope of the fitted lines
size=4; %correcting unit factor
s1=D(1)*10^size;
s2=E(1)*10^size;
s3=F(1)*10^size;
s4=G(1)*10^size;
s5=H(1)*10^size;
s6=I(1)*10^size;
slopes=[s1;s2;s3;s4;s5;s6];
clear D E F G H I %memory management
%% determining the pixel shift based on the data finding the
sensitivity
%of slope to pixel shift the equation of the slope ofthe trend is
%y=.0011x
slopefit=.0011; %sensitivity factor of theta/sub-pixel shift
shift0=0; %don't shift 0
shift1=round((atand(s1)/slopefit)); %amount to shift 1
shift2=round((atand(s2)/slopefit)); %amount to shift 2
shift3=round((atand(s3)/slopefit)); %amount to shift 3
shift4=round((atand(s4)/slopefit)); %amount to shift 4
shift5=round((atand(s5)/slopefit)); %amount to shift 5
shift6=round((atand(s6)/slopefit)); %amount to shift 6
shift123456=[shift1;shift2;shift3;shift4;shift5;shift6];
clear s1 s2 s3 s4 s5 s6 % memory management
%% Final plotting of shifted data
p0fin=circshift(p0i,[0 shift0]); %rotating vector by shift amount
p1fin=circshift(p1i,[0 shift1]); %rotating vector by shift amount
p2fin=circshift(p2i,[0 shift2]); %rotating vector by shift amount
p3fin=circshift(p3i,[0 shift3]); %rotating vector by shift amount
p4fin=circshift(p4i,[0 shift4]); %rotating vector by shift amount
p5fin=circshift(p5i,[0 shift5]); %rotating vector by shift amount
p6fin=circshift(p6i,[0 shift6]); %rotating vector by shift amount
file='After_alignement_plunges.mat';
save(file,'xint','p0fin','p1fin','p2fin','p3fin','p4fin','p5fin','p6fin
');
clear shift1 shift2 shift3 shift4 shift5 shift6
%% Subtracting The intial plunge giving the residuals
p0i=p0fin;
p0n=p0i-p0i; %after fine alignment correction for tool shape
p1fins=p1fin-p0i; %after fine alignment correction for tool shape
p2fins=p2fin-p0i; %after fine alignment correction for tool shape
p3fins=p3fin-p0i; %after fine alignment correction for tool shape
p4fins=p4fin-p0i; %after fine alignment correction for tool shape

```

```

p5fins=p5fin-p0i; %after fine alignment correction for tool shape
p6fins=p6fin-p0i; %after fine alignment correction for tool shape
clear p1fin p2fin p3fin p4fin p5fin p6fin
%% moving to zero
p1finf=p1fins-nanmean(p1fins(lfit:rfit)); %removing DC offset in
residuals
p2finf=p2fins-nanmean(p2fins(lfit:rfit)); %removing DC offset in
residuals
p3finf=p3fins-nanmean(p3fins(lfit:rfit)); %removing DC offset in
residuals
p4finf=p4fins-nanmean(p4fins(lfit:rfit)); %removing DC offset in
residuals
p5finf=p5fins-nanmean(p5fins(lfit:rfit)); %removing DC offset in
residuals
p6finf=p6fins-nanmean(p6fins(lfit:rfit)); %removing DC offset in
residuals
shift=max(abs(shift123456)); %greatest amount shifted
p0n=p0n(2*shift:end-2*shift); %removing the shifted values from vector
p1finf=p1finf(2*shift:end-2*shift); %removing the shifted values from
vector
p2finf=p2finf(2*shift:end-2*shift); %removing the shifted values from
vector
p3finf=p3finf(2*shift:end-2*shift); %removing the shifted values from
vector
p4finf=p4finf(2*shift:end-2*shift); %removing the shifted values from
vector
p5finf=p5finf(2*shift:end-2*shift); %removing the shifted values from
vector
p6finf=p6finf(2*shift:end-2*shift); %removing the shifted values from
vector
xint=xint(2*shift:end-2*shift); %x-vector of shift removed residuals
clear p1fins p2fins p3fins p4fins p5fins p6fins
%% Residual final plot
figure
plot(xint,p0n)
hold on
plot(xint,p1finf)
plot(xint,p2finf,'r')
plot(xint,p3finf,'k')
plot(xint,p4finf,'g')
plot(xint,p5finf,'c')
plot(xint,p6finf,'m')
title('Monel Short 1000RPM F2')
ylabel('Edge Recession of Diamond, (\mum)')
xlabel('Plunge Position, (\mum)')
ylim([-0.1 0.3])
legend('Baseline','Residual 1','Residual 2','Residual 3','Residual
4',...
'Residual 5','Residual 6','Location','Best')
file='Data_processed_RESIDUALS.mat';
save(file,'xint','p0n','p1finf','p2finf','p3finf','p4finf','p5finf','p6
finf');

```